Rock Mechanics and Rock Engineering
https://doi.org/10.1007/s00603-020-02179-z

ORIGINAL PAPER

A New Criterion for Numerical Modelling of Hangingwall Overbreak in Open Stopes

J. A. Vallejos[1] · L. Díaz[1]

Received: 11 January 2019 / Accepted: 17 June 2020
© Springer-Verlag GmbH Austria, part of Springer Nature 2020

Abstract

Determining stability, quantifying planned dilution, and estimating the potential dilution associated with hangingwall overbreak are critical in the process of stope design in sublevel open stoping mines. To satisfy these objectives, empirical stability graphs and numerical modelling are currently used in the mining industry. Empirical methods are limited to the database used to calibrate them. In the case of numerical modelling, some of the available criteria used to evaluate hangingwall overbreak do not include the intermediate principal stress around the stope and/or the rock mass geotechnical characteristics. In this study, a new criterion for numerical modelling is proposed to estimate the hangingwall overbreak in open stopes. This new criterion includes the intermediate principal stress around the stope and the rock mass geotechnical characteristics. To develop the criterion, several open stope numerical models are simulated considering different geometrical and geotechnical conditions. The criterion is calibrated to reproduce empirical case histories of hangingwall overbreak. Next, the criterion is verified with case histories of hangingwall overbreak that presented different conditions used to calibrate the criterion. The proposed criterion establish a significant influence and relationship between rock quality and the minimum and intermediate principal stresses on hangingwall overbreak. The criterion offers sufficient flexibility for application to a wide range of geometries, in situ stress conditions, and depth and rock mass properties.

Keywords Open stopes · Numerical modelling · Hangingwall overbreak · Stress distribution

List of Symbols

HR	Hydraulic radius [m]
RQD	Rock quality designation
J_n	Joint set number
J_r	Joint roughness number
J_a	Joint alteration number
Q'	Rock tunneling quality index modified
A	Stress factor
B	Joint adjustment orientation factor
C	Gravity factor
N	Mathews stability number
H	Hangingwall height [m]
L	Hangingwall length [m]
GSI	Geological strength index
E_i	Intact rock Young's modulus [GPa]
E_{rm}	Rock mass Young's modulus [GPa]
D	Factor of disturbance
σ_t	Tensile strength [MPa]
s	Rock mass constant, Hoek and Brown failure criterion
σ_c	Uniaxial compressive strength [MPa]
m_i	Intact material constant, Hoek and Brown failure criterion
m_b	Reduced value of the material constant, Hoek and Brown failure criterion
σ_1	Major principal stress [MPa] (positive in compression)
σ_2	Intermediate principal stress [MPa] (positive in compression)
σ_3	Minimum principal stress [MPa] (positive in compression)
z	Stope depth [m]
p	Mean principal stress [MPa]
b	Differential stress ratio
RSS	Residual sum of squares
n	Total number of simulated cases
y_i	Minimum principal stress of the simulated cases considering empirical ELOS [MPa]

✉ L. Díaz
javallej@ing.uchile.cl

[1] Department of Mining Engineering, Advanced Mining Technology Center (AMTC), University of Chile, Santiago, Chile

Published online: 04 July 2020

$\hat{y}_i$	Minimum principal stress estimated by the evaluated criterion [MPa]
R^2	Coefficient of determination
$\bar{R}^2$	Adjusted coefficient of determination
k	Number of independent variables
$\bar{y}$	Average value of minimum principal stress of the simulated cases [MPa]

1 Introduction

Stope design is a unique process that considers the mining sequence, stable geometry, space between levels, and support and filling requirements. When comparing different options for stope design, it is important to evaluate them in terms of cost and production, as well as in terms of stope stability and the potential dilution associated with walls. It has been established that the main mechanism that allows quantification of the dilution in sublevel stoping corresponds to wall overbreak (Cepuritis and Villaescusa 2006).

Quantifying the dilution requires the implementation of the cavity monitoring system (CMS) and subsequent comparative analyses. However, according to the level of dilution certainty, it is possible to distinguish between planned dilution and unplanned dilution (Scoble and Moss 1994). Planned dilution is defined in the design of a basic unit; hence, the challenge is in estimating the unplanned dilution, characterized mainly by the amount of hangingwall overbreak. Quantifying the unplanned dilution allows updating the tonnage to extract its grade and the processing value, which allows a higher level of certainty of the reserves available for mining planning and better control of the production costs.

Empirical design methods are widely used as a simple means of generating broad design guidelines for primary stopes (Henning and Mitri 2008). Mathews et al. (1981) developed the first empirical stope stability graph, which became popular through the expansion of the database from 50 case histories to 176 case histories by Potvin (1988). Trueman et al. (2000), Mawdesley et al. (2001) and Mawdesley (2002) extended the original Mathews stability graph by increasing the number of case histories from 176 to 485 for 38 mines in North America, Australia, Chile, and England.

The stability graph method is based on a relationship between the hydraulic radius (HR) and the stability number, N. The hydraulic radius accounts for the stope geometry face and is defined by (Laubscher and Taylor 1976):

$$\mathrm{HR} = \frac{\text{Stope face area}}{\text{Stope face perimeter}}. \tag{1}$$

The Mathews stability number, N, is defined by:

$$N = Q' \times A \times B \times C, \tag{2}$$

where Q' is defined by (Mathews et al. 1981):

$$Q' = \frac{RQD \times J_r}{J_n \times J_a}. \tag{3}$$

where RQD (Deere et al. 1967) is the rock quality designation, J_n is the joint set number, J_r is the joint roughness number, and J_a is the joint alteration number. In Eq. (2), A, B, and C are defined as the stress factor, the t adjustment orientation factor, and the gravity factor, respectively.

Several authors have worked at improving the reliability of the stability graph predicting open stope performance. The most significant limitations are the following (Suorineni 2010):

- The subjectivity in the definition of the stability zones.
- The absence of standardization of the extended database.
- The non-representation of the rock stress factor, A, for instabilities caused by low confinement conditions.
- The poor representation of the sliding failure modes by the gravity adjustment factor C.

In the past 3 decades, several studies have focused on eliminating the effects of these constraints. The developments have resulted in different values of the stability number, N, for the same stope surface and different stability zones, and have resulted in different models for estimating the hangingwall overbreak (Suorineni 2010).

Several modifications and updates to the A, B, and C factors have been proposed (Hadjigeorgiou et al. 1995; Clark and Pakalnis 1997; Diederichs and Kaiser 1999; Stewart and Trueman 2004; Bewick and Kaiser 2009; Mitri et al. 2011; Vallejos et al. 2016, 2017a). However, most of these studies have not evaluated the impact of the proposed modifications on the performance of the method. Other authors have proposed new factors that modify the stability number according to the time effect in the excavation (T) (Pakalnis 1986; Tannant and Diederichs 1997) and the influence of faults on stope stability (F) (Suorineni et al. 2001), but these factors have generally not been applied.

The ability of the CMS to produce a three-dimensional study of a stope enabled Clark and Pakalnis (1997) to develop the concept of equivalent linear overbreak/slough (ELOS) to estimate the dilution of an excavation. Different authors have proposed the use of dilution lines (Scoble and Moss 1994; Papaioanou and Suorineni 2015; Suorineni et al. 2016) and ELOS lines (Clark 1998) in the stability graph method. Figure 1 presents an updated ELOS chart developed by Castro (2015) based on 307 case histories of unsupported open stope walls from Canadian mines and the addition of

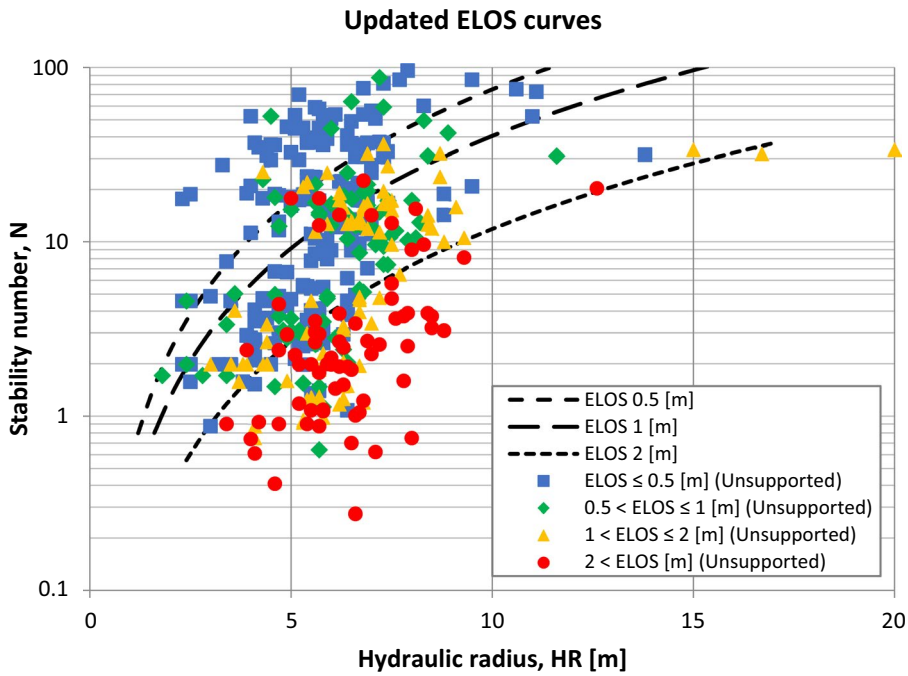

Fig. 1 Updated ELOS curves (Castro 2015)

38 new case histories from two Chilean mines. In these types of databases, it is necessary to consider the geological and operational conditions under which the curves were developed to use them properly. Therefore, to improve the performance of the stability graph method, the MineRoc® software (Vallejos et al. 2015) was developed as a support tool for open stope design. This software allows storing all the information related to the stope overbreak case histories of a site in a single platform, which ensures the possibility of improving the performance of the local stability curves (Vallejos et al. 2017b).

Continuum numerical modelling has become predominant in the mining industry to analyse the stability and estimate the overbreak in stope walls (Jing 2003). Mitri et al. (1998) mentioned that a simple criterion of stress confinement (minimum principal stress, σ_3) can be used to evaluate the stability and potential dilution of the stope hangingwall. Following this idea, several authors (Clark 1998; Suorineni 1998; Diederichs and Kaiser 1999; Henning and Mitri 1999; Martin et al. 1999; Henning and Mitri 2007; Amoussou et. 2020) have shown that stress relaxation, low stress, and/or tensile stress have negative effects on stope stability, and have established that criteria such as $\sigma_3 \leq 0.2$ [MPa], $\sigma_3 = 0$ [MPa] and $\sigma_3 = \sigma_t$ (tensile strength) work properly in certain cases to estimate the dilution of the excavation. Stewart and Trueman (2003) developed a study in which they suggested that the amount of stress relaxation, defined by the total relaxation (σ_3 and $\sigma_2 \leq 0.2$ [MPa]) and tangential relaxation (one principal stress < 0.2 [MPa] and less than 20° inclination with respect to the wall), impacts hangingwall stability, indicating that two-dimensional modelling is insufficient to determine whether the surface of an excavation is relaxed. Stewart and Trueman (2004) concluded that in discontinuous rocks, the intermediate principal stress (σ_2) of the wall can influence the stope stability when the minimum principal stress (σ_3) is tensile.

The effects of the stope geometrical parameters on stope stability have been investigated in several studies. The effect of the open stope height on stability was studied by Chen et al. (1983), Yao et al. (1999), and Henning (2007). These studies indicated that increasing the stope height results in increasing the overbreak of stope walls. The effect of stope strike length variations on stability was studied by Henning and Mitri (2007) and Hughes (2011), who showed that longer strike lengths increase the stope overbreak more than shorter strike lengths do. Studies on the effect of the stope span width on stability have demonstrated that a decreased stope span width increases the stope dilution (Pakalnis et al. 1996; El Mouhabbis 2013). The effect of stope hangingwall dip on stope stability has also been studied (Henning and Mitri 1999; Yao et al. 1999; Hughes 2011). These studies concluded that a lower hangingwall dip contributes to a larger overbreak due to the significant effect of gravity on the hangingwall. The effect of the hangingwall size and shape defined by the hydraulic radius on stope stability was assessed by Clark (1998) and Wang et al. (2007). These studies showed that increasing the hydraulic radius of the hangingwall increases the stope overbreak and, therefore, increases the instability of the stope. Recently, Heidarzadeh et al. (2018) studied the individual and combined effects of stope geometrical parameters

(hangingwall hydraulic radius, stope span width, and stope hangingwall dip) on the probability of stope failure. The results indicate that the interaction between the parameters modifies the way that each parameter affects the probability of stope failure; therefore, the effect of each geometrical parameter on the probability of failure must be assessed by considering the level of variation in other parameters.

Sainsbury et al. (2015) used discrete analysis to model stope geometries to provide a quantitative assessment of the expected dilution in the stope hangingwall and crown. In this study, the authors compared the expected ELOS estimated through empirical design methods with the ELOS calculated using discrete numerical modelling. The dilution volume in these models was calculated by adding up all the zone volumes that had a displacement greater than 1 [m], a velocity greater than 1e−6 [m/s], and a volumetric strain greater than 3%. The results indicated that the numerical methods were able to accurately capture the hangingwall failure that was not predicted by the empirical design methods and to provide a more quantitative and robust prediction of the crown instability. However, three-dimensional discrete analysis simulations are not expected to be used routinely in conceptual studies but are suggested to be used in the early to late stages of development of a stoping operation when significant rock mass data sets are available to provide design reliabilities of more than 80%.

The most significant empirical and numerical developments for estimating the stability and dilution in open stopes are chronicled in Fig. 2. Based on Fig. 2, the most relevant studies that have modified the rock stress factor (A) are Stewart and Trueman (2004), Mitri et al. (2011), and Vallejos et al. (2016). Stewart and Trueman (2004) used three-dimensional numerical models for a number of stope surfaces that exhibited tensile stresses. They highlighted that when the minor principal stress is negative, the intermediate principal stress significantly affects the rock mass behaviour. Their study concluded that when the intermediate principal stress is positive, then $A = 1$ is appropriate. When the principal stress is also negative, then $A = 0.7$ should be used. These conclusions were established with limited case studies. Mitri et al. (2011) proposed a new rock stress factor that reflects the impact of low confinement on the stability of walls. These authors did not provide statistical evidence of the performance of the new factor on the empirical databases. Vallejos et al. (2016) evaluated the impact of different rock stress factors on the performance of the empirical stability graph. They proposed a new rock stress factor for high-stress conditions.

To investigate the impact of these updates of the stability graph method, an empirical database that includes the complete stress tensor estimated at the walls of the stopes must be used. Given that this is not currently available, in this study, the original rock stress factor proposed

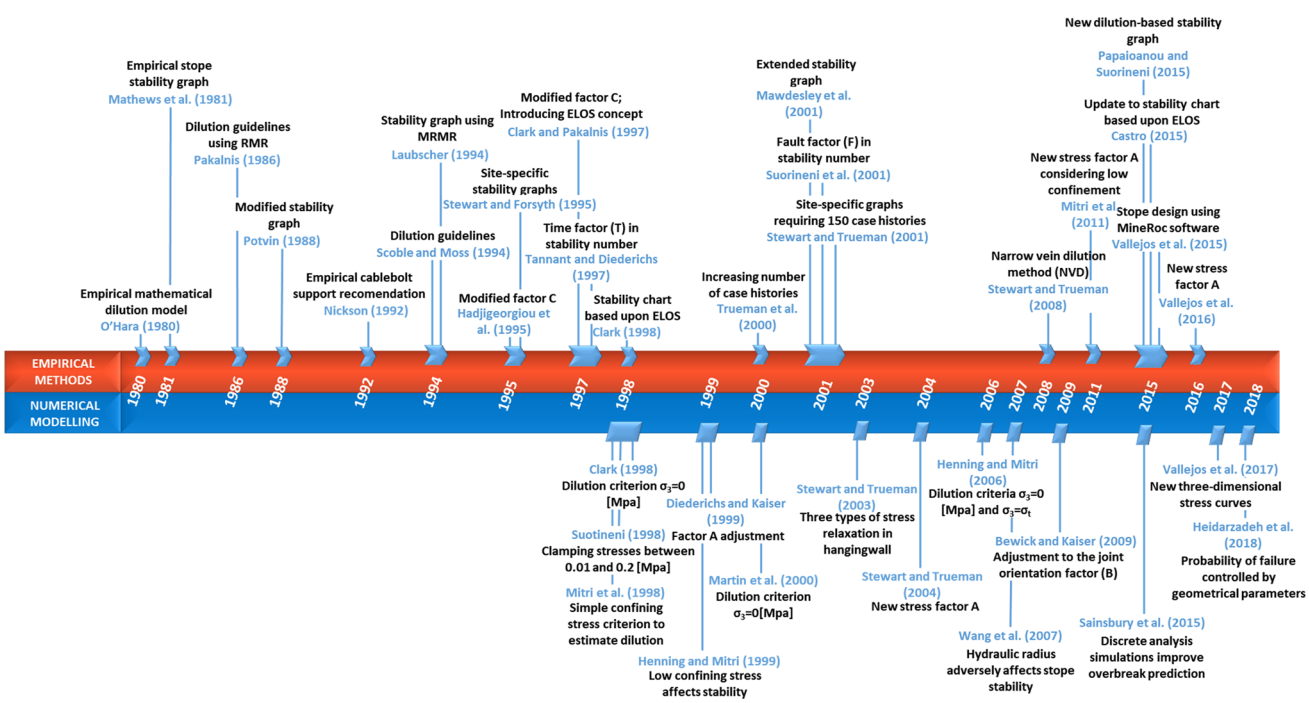

Fig. 2 Timeline describing the main works that used empirical methodologies and numerical modelling to estimate open stope stability and overbreak, adapted from Díaz et al. (2018)

by Mathews/Potvin is employed as a reference for the development of the overbreak criterion.

Díaz et al. (2018) studied, through three-dimensional continuum numerical modelling (FLAC3D v6, Itasca Consulting Group 2018), the performance of the conventional criteria mentioned above ($\sigma_3 = 0$ [MPa] and $\sigma_3 = \sigma_t$) using the case history database from Canada and the updated ELOS curves (Fig. 1). In that study, 56 cases were simulated in terms of the hydraulic radius and Mathews stability number, *N*, represented by the ordered pair (HR, *N*). In each simulation, the corresponding volume of the isocontour that defines each criterion was estimated and associated with the hangingwall. Therefore, for each stability number, the ELOS obtained by the simulation was compared to the empirical ELOS.

Figure 3 presents a comparison between the empirical ELOS curves and the estimated values from numerical modelling using both criteria. Each dot in Fig. 3 represents the results from numerical modelling, while the dotted lines represent the updated empirical curves. These graphs indicate that there is no good correlation between the empirical ELOS guidelines and the estimated overbreak from the studied numerical modelling criteria. This observation is related to the fact that the criteria do not consider certain parameters that influence the hangingwall stability, such as rock mass quality and stress relaxation. Therefore, it is necessary to propose an improved criterion that includes the rock mass quality and stress relaxation around the excavation using the empirical ELOS curves as a guide. This proposal is the main scope of this study.

2 Modelling considerations

In this paper, three-dimensional finite-difference continuum modelling (FLAC3D v6, Itasca Consulting Group 2018) is used to calibrate and verify a new criterion to estimate hangingwall overbreak. Models are simulated using this software because of the flexibility that it provides using the FISH programming language. Several cases are modelled considering different geometrical and geotechnical parameters. The following sections summarize the modelling methodology, including the empirical database, geometrical considerations, constitutive model, in situ stresses, boundary conditions, and model outputs.

2.1 Empirical database

To establish the representative cases for the numerical models, 582 case histories of sublevel stoping mining in Canada were collected from the literature (Table 1) (Mah 1997; Clark 1998; Wang et al. 2003; Capes 2009). The database includes information on hangingwalls (HWs) and footwalls (FWs), not including information on backs or end walls.

Table 1 Sublevel stoping database by author

Authors	Number of cases	Mining method	Source
Mah (1997)	103	Sublevel Stoping	Canada
Clark (1999)	102	Sublevel Stoping	Canada
Wang et al. (2003)	149	Sublevel Stoping	Canada
Capes (2009)	228	Sublevel Stoping	Canada, Australia

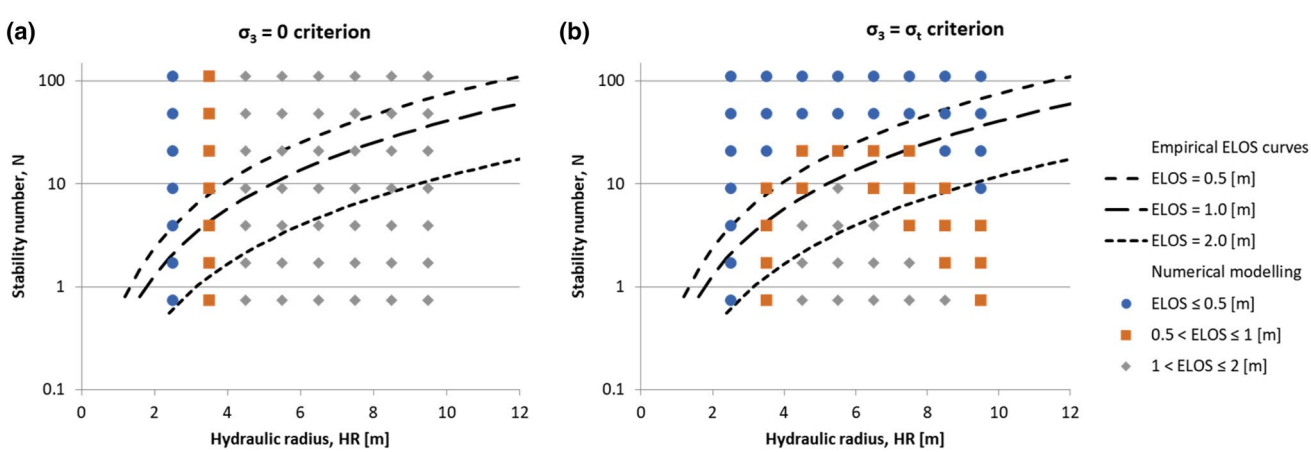

Fig. 3 Comparison between the updated empirical ELOS curves and the estimated values from three-dimensional numerical modelling using literature criteria, adapted from Díaz et al. (2018). (**a**) $\sigma_3 = 0$ criterion, and (**b**) $\sigma_3 = \sigma_t$ criterion. Dots represent the results from numerical modelling, and dotted lines represent the updated empirical curves

Table 2 Minimum and maximum values of the parameters considered in the collected hangingwall empirical database used for the development of the overbreak criterion (307 cases)

Parameter	Min	Max
Depth [m]	75.0	1070.0
Dip [°]	23.0	90.0
Width [m]	1.4	52.0
Length [m]	5.5	60.0
Height [m]	10.0	124.0
Aspect ratio (height/length)	0.4	7.4
HR [m]	1.8	21.2
Q'	0.4	33.8
N	0.8	137.5

The available information of hangingwalls is considered to establish a database of case histories and for further development of the overbreak criterion. In addition, footwalls with dips greater than or equal to 85° are included in the database.

As an additional filter, only stopes walls without support or reinforcement are considered. Finally, the database contains 307 case histories of hangingwalls without support. This filtered database is used as a reference to model the cases studied in this paper. Table 2 shows the minimum and maximum values of the parameters considered in the filtered empirical database.

Unfortunately, the empirical collected database does not include the complete information of all the required variables, especially those related to rock mass properties, depth, and stress condition. Therefore, representative values have been adopted. In the following sections, the modelling cases are presented.

2.2 Definition of modelling cases

Different stopes were modelled using the database shown in Table 2 and the updated empirical overbreak guide (Fig. 1). Each ELOS curve (ELOS of 0.5, 1, and 2 [m]) was discretized into 17 points, representing 17 ordered pairs (HR, N) with different hangingwall sizes, the values of which vary between HR = 3 [m] and HR = 11 [m] (Fig. 4). For each hydraulic radius, there is a stability number that is decomposed to obtain the Q' value (Eq. 4):

$$Q' = \frac{N}{A \times B \times C}. \tag{4}$$

The Q' value is related to the geological strength index (GSI) system used to estimate the geotechnical parameters of the rock mass. Each of the three curves presented has 17 cases (HR, Q', and ELOS) that were simulated in terms of the size of the stope, the rock mass characterization, and the amount of the expected overbreak.

Additionally, a variation in the aspect ratio of the hangingwall stope (Height/Length) is considered to represent the geometry in a better manner. Figure 5 shows the distribution of the aspect ratio present in the empirical database. To represent 90% of the population, eight values were selected: 0.5, 0.8, 1.2, 1.6, 2.0, 2.4, 2.8, and 3.1. The value of 1.6 represents the average of the empirical database. In this manner, with 17 cases for three ELOS curves and eight aspect ratios, a total of 408 cases must be modelled numerically.

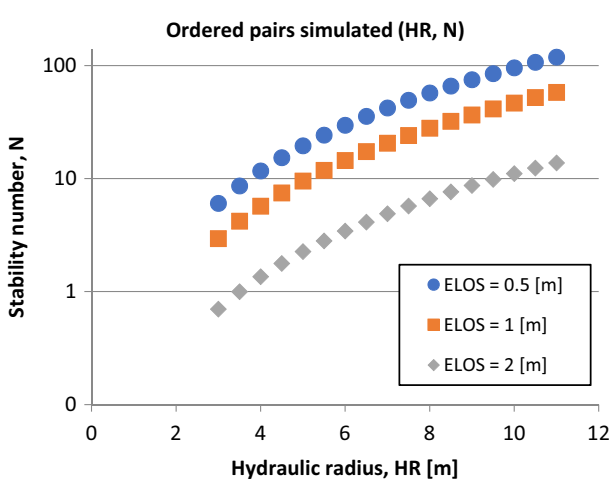

Fig. 4 Discretization of the updated empirical ELOS curve for numerical modelling

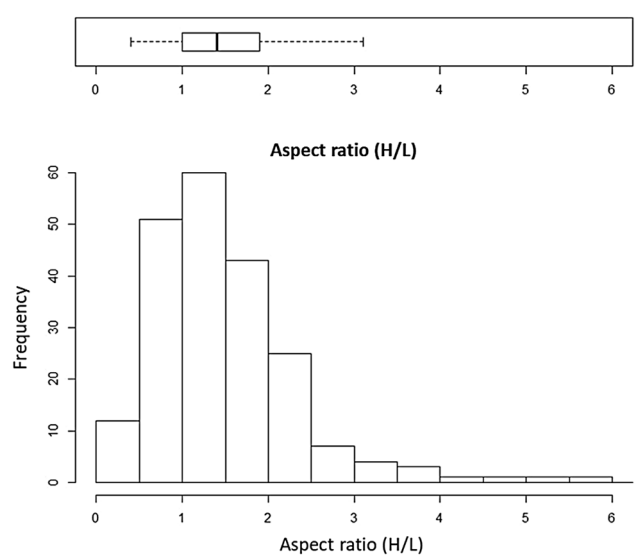

Fig. 5 Distributions of the ratio between the height and length of the hangingwall stope available in the empirical database

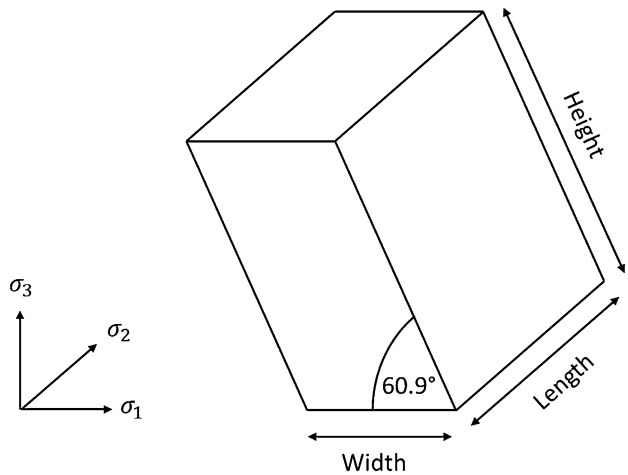

Fig. 6 Definition of stope geometry and principal in situ stress orientations for numerical modelling

2.2.1 Geometry

The following modelling considerations are included (Fig. 6):

- The stopes are considered isolated excavations.
- The width of the stopes is equal to 7.2 [m] according to the average value of the database.
- The dip of the stope walls is equal to 60.9° according to the average value of the database.
- The depth of the stopes is equal to 778.4 [m] according to the average value of the database.
- The size of the model is ten times larger than the stope width, length, and height to eliminate the boundary effects.
- The boundary conditions applied to the model consider that the right and left boundaries are bound to a displacement restriction in the x direction, the front and back boundaries, in the y direction, and the top and bottom boundaries, in the z direction.
- Based on a mesh sensitivity study, the selected mesh size at the edge of the stopes is 0.8 [m] and increases as one moves away from the excavation.
- The major principal stress is considered perpendicular to the strike of the hangingwall; the intermediate principal stress is considered parallel to the strike of the hangingwall; and the minimum principal stress is considered vertical.
- The aspect ratio (H/L) values are 0.5, 0.8, 1.2, 1.6, 2.0, 2.4, 2.8, and 3.1.
- The hydraulic radius (HR) is calculated according to the ordered pair simulation.
- The hydraulic radius and aspect ratio are known variables, so it is possible to calculate the height and length values of the hangingwall according to Eq. (5):

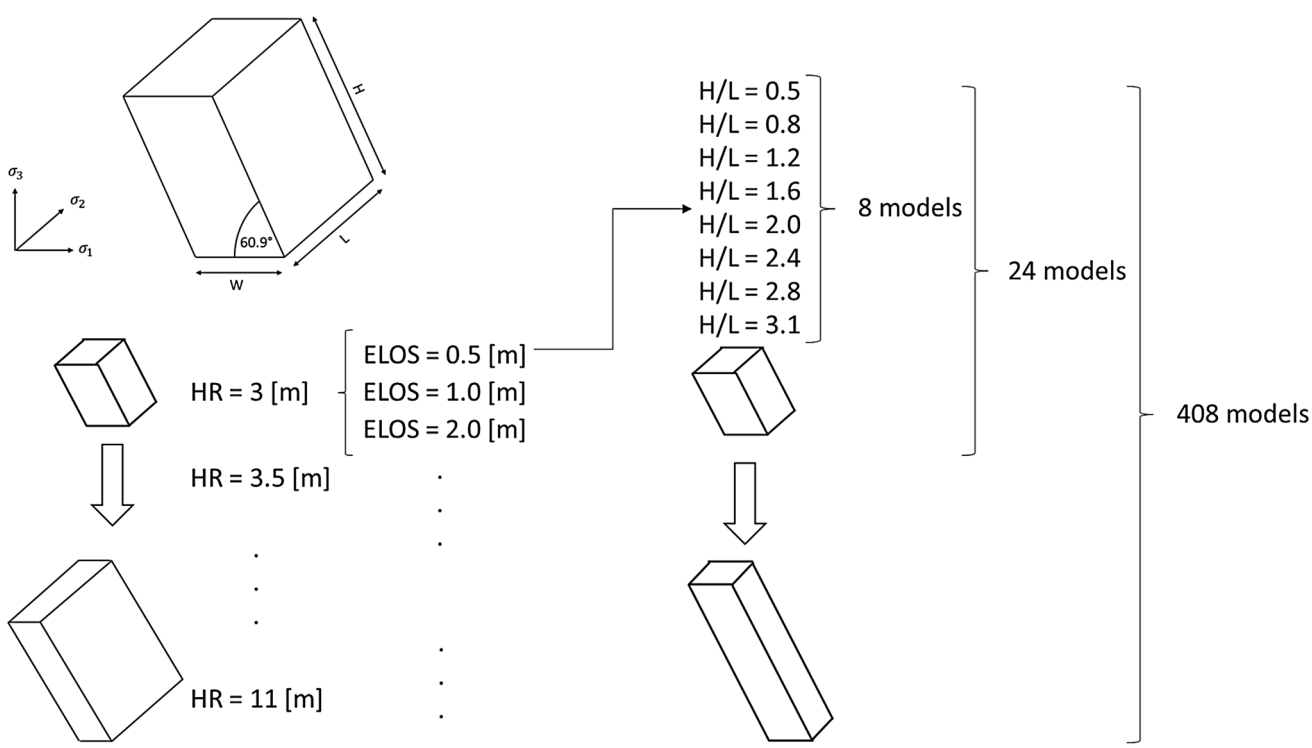

Fig. 7 Methodology followed to define the 408 models for the analysis

$$H = 2 \bullet HR \bullet \left(\frac{H}{L} + 1\right) \quad L = \frac{H}{\left(\frac{H}{L}\right)}. \tag{5}$$

Figure 7 shows the methodology followed to define the 408 models for the analysis.

2.2.2 Constitutive model

The empirical collected database does not include enough information to establish the peak and post-peak parameters. The results of plastic modelling depend on the selected parameters and mesh density. To establish reliable results using plastic models, it is necessary to have the plastic parameters for each site and case. Considering that the stability graph method uses stresses estimated by linear-elastic models and that several authors have estimated dilution from the hangingwall based on linear-elastic models (Clark 1998; Suorineni 1998; Diederichs and Kaiser 1999; Henning and Mitri 1999, 2007; Martin et al. 1999; Stewart and Trueman 2003; Heidarzadeh et al. 2018), a linear-elastic approach was adopted. This also provides a criterion that can be used in practice and be useful for the mining industry.

2.2.3 Rock mass parameters

The rock mass classification varied in each case according to the value of the stability number N indicated in the ordered pair. Through the value of the adjustment factors of the Mathews stability method, the rock mass classification is estimated by the Q' system. This estimation is possible; since all the hangingwall case histories from the database presented $A = 1$, the discontinuity factor is considered equal to $B = 0.5$ given that 98% of the cases of the database presented this value, and the dip of the stopes is constant ($C = 4.6$). To estimate the rock mass classification GSI, first, the rock mass is assumed to be completely dry, and the joint orientation adjustment is equal to zero. With these assumptions, the GSI is related to RMR_{1976} according to Eq. (6) (Hoek et al. 1995):

$$\mathrm{GSI} = \mathrm{RMR}_{1976}. \tag{6}$$

Then, the rock mass classification GSI is estimated according to Eq. (7) (Hoek et al. 1995):

$$\mathrm{GSI} = 9\ln\left(Q'\right) + 44. \tag{7}$$

For the numerical modelling, a linear-elastic constitutive model is considered, defined by the Young's modulus (E_i) and Poisson's ratio (ν) of the rock mass. Intact elastic parameters were obtained from the average of the database (Table 3), and the rock mass modulus was estimated from Eq. (8) (Hoek and Diederichs 2006):

$$E_{\mathrm{rm}} = E_i\left(0.02 + \frac{1 - \frac{D}{2}}{1 + e^{\frac{60+15D-\mathrm{GSI}}{11}}}\right), \tag{8}$$

where E_{rm} is the rock mass deformation modulus, E_i is the intact rock deformation modulus, GSI is the geological strength index, and D is the disturbance factor. In this study, the value of the disturbance factor is assumed to be equal to 0.

The tensile strength is calculated using the Hoek–Brown failure criterion (Eq. 9) (Hoek et al. 2002):

$$\sigma_t = -\frac{s \bullet \sigma_c}{m_b}, \tag{9}$$

where s is a constant for the rock mass given by Eq. (10), σ_c is the uniaxial compressive strength of the intact rock material, and m_b is a reduced value of the material constant m_i given by Eq. (11):

$$s = \exp\left(\frac{\mathrm{GSI} - 100}{9 - 3D}\right). \tag{10}$$

$$m_b = m_i \bullet \exp\left(\frac{\mathrm{GSI} - 100}{28 - 14D}\right). \tag{11}$$

2.2.4 In situ stresses

Due to the absence of specific information associated with the magnitude and orientation of the principal stresses in the database, the in situ stresses estimated by Maloney et al. (2006) and Arjang (1989) for Canada are used (Eq. 12):

$$\sigma_1 = 23.64 + 0.026 \bullet z[MPa]$$

$$\sigma_2 = 17.10 + 0.016 \bullet z[MPa], \tag{12}$$

$$\sigma_2 = 17.10 + 0.016 \bullet z[MPa]$$

Using the average depth of the empirical database (z = 778.4 [m]), the major principal stress is considered perpendicular to the strike of the hangingwall and equal to 43.9 [MPa], the intermediate principal stress is considered parallel to the strike of the hangingwall and equal to 29.6

Table 3 Average intact rock parameters

Intact rock parameters	
σc [MPa]	157
mi	13
E_i [GPa]	57
ν	0.3

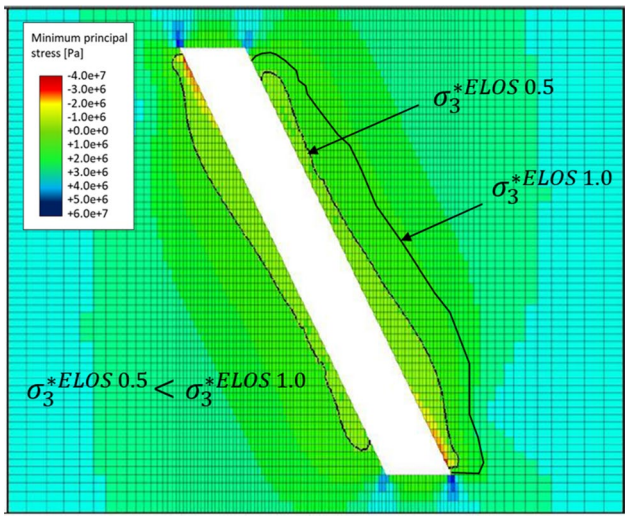

Fig. 8 Example of σ_3 isocontours obtained from numerical models that reproduce different values of the empirical ELOS

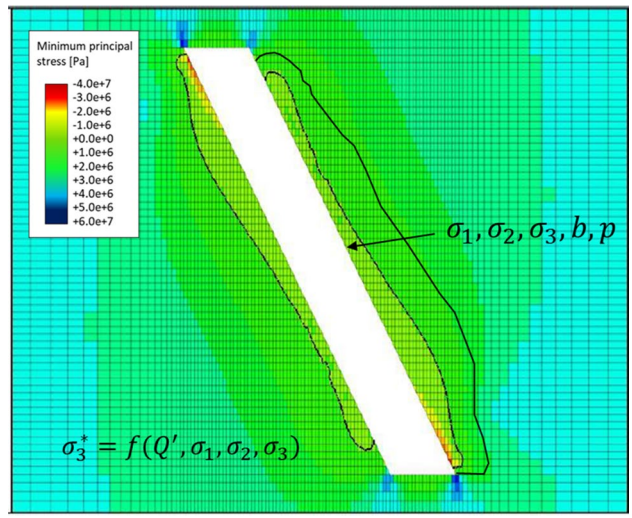

Fig. 9 Major (σ_1), intermediate (σ_2), and minor (σ_3) principal stresses obtained from the three-dimensional continuum numerical model for each stope hangingwall geometry

[MPa], and the minimum principal stress is considered vertical and equal to 16.6 [MPa].

2.3 Output model variables

Given the geometry of the stope and the rock mass quality Q' for each numerical modelling case, the following output variables were considered (Fig. 8). The minimum principal stress isocontour, σ_3, that represents the rock mass volume corresponding to the empirical ELOS is estimated and indicated by σ_3^*. The σ_3^* value is calculated using a user-developed code. This function iterates the σ_3 value in intervals of 0.0001 [MPa], calculates for each σ_3 the volume within the isocontour, and determines the numerical overbreak values to compare with the empirical ELOS target value. When the difference between the simulated value of the ELOS and the target value of the empirical ELOS does not exceed a tolerance of 0.005 [m], the iteration ends. The last σ_3 value used in the iteration is set and indicated by σ_3^*. Figure 8 shows an example of two σ_3 isocontours that reproduce different empirical ELOS values.

Major (σ_1), intermediate (σ_2), and minor (σ_3) principal stress values are obtained at the centre of the stope hangingwall, as shown in Fig. 9. This is done to relate the three-dimensional principal stress condition in the hangingwall with the stress relaxation isocontour (σ_3^*) and, therefore, with the stability of the stope wall (Clark and Pakalnis 1997; Clark 1998; Suorineni 1998; Diederichs and Kaiser 1999; Henning and Mitri 1999, 2007; Martin et al. 1999; Wang et al. 2002; Stewart and Trueman 2003, 2004). The σ_1, σ_2 and σ_3 values are used to calculate the mean principal stress (p) and the differential stress ratio (b) according to Eq. (13) to quantify the effect of the intermediate stress on stope stability (Stewart and Trueman 2004).

$$p = \frac{\sigma_1 + \sigma_2 + \sigma_3}{3} \quad b = \frac{\sigma_2 - \sigma_3}{\sigma_1 - \sigma_3}. \tag{13}$$

3 Results

In this section, the results are processed and used to propose several candidate overbreak criteria. Next, the overbreak criteria are calibrated. The sensitivity of the results to the mesh is evaluated. Finally, the performance of the criteria is evaluated, and a new criterion to estimate hangingwall overbreak is proposed.

3.1 Calibration of overbreak criteria

Using the principal stress values (σ_1, σ_2, σ_3) obtained at the centre of the stope hangingwall, the rock mass quality (Q'), and the minimum principal stress isocontour (σ_3^*) that represents the empirical ELOS, the criteria to estimate the hangingwall overbreak are established through statistical optimization.

The following considerations are established regarding the considered variables and overbreak criteria:

- The dependent variable of each criterion is σ_3^* measured in [MPa].
- The variable related to the quality of the rock mass (Q') must be present in each of the proposed criteria since the overbreak appears to be rock mass dependent (Stewart 2005).
- The other independent variables of each criterion could be σ_1, σ_2, σ_3, b, and/or p.
- Given the lognormal behaviour of Q', it is considered that this parameter can be used logarithmically.
- The following approach is used to assess the presence of correlation (Larose 2006): $|\rho| > 0.7$, the variables are correlated; $0.33 \leq |\rho| \leq 0.7$, the variables are slightly correlated; and $|\rho| < 0.33$, the variables are not correlated, where ρ is the correlation coefficient.

Table 4 presents the correlation coefficients between the considered variables, used to propose several candidate criteria to estimate the hangingwall overbreak.

Table 4 has the following implications:

- Q' has no correlation with the variables σ_2, σ_3 and b,
- Q' is slightly correlated with the variables σ_1 and p, and
- σ_3 has no correlation with Q', σ_1 and b.

These implications are important to consider, because the performance of each criterion can be influenced by the correlation that exists between the independent variables.

Based on the above-mentioned analysis, Table 5 shows the proposed criteria candidates for estimating the hangingwall overbreak considering the geotechnical characteristics of the rock mass (Q') and principal stresses at the stope hangingwall, in addition to the variables b and p. It should be noted that the principal stresses must be in [MPa] to prevent unit problems in the criteria and that the parameters a, b', c, and d are considered constant in each criterion. The conventional criteria ($\sigma_3 = 0$ [MPa] and $\sigma_3 = \sigma_t$) are also included for comparison purposes.

To calibrate the parameters of each criterion, the least-squares method is used. This method involves selecting the parameters that minimize the following residual sum of squares (RSS) (Eq. 14):

Table 5 Proposed criteria candidates to estimate hangingwall overbreak

Criterion number	Criterion	Number of independent variables
0a	$\sigma_3^*[\text{MPa}] = 0$	0
0b	$\sigma_3^*[\text{MPa}] = \sigma_{t-\text{average}}$	1
1	$\sigma_3^*[\text{MPa}] = a + b' \bullet \log(Q')$	1
2	$\sigma_3^*[\text{MPa}] = a + b' \bullet \log(Q') + c \bullet \sigma_1$	2
3	$\sigma_3^*[\text{MPa}] = a + b' \bullet \log(Q') + c \bullet \sigma_2$	2
4	$\sigma_3^*[\text{MPa}] = a + b' \bullet \log(Q') + c \bullet \sigma_3$	2
5	$\sigma_3^*[\text{MPa}] = a + b' \bullet \log(Q') + c \bullet \sigma_1 + d \bullet \sigma_3$	3
6	$\sigma_3^*[\text{MPa}] = a + b' \bullet \log(Q') + c \bullet b$	3
7	$\sigma_3^*[\text{MPa}] = a + b' \bullet \log(Q') + c \bullet \log(p)$	3
8	$\sigma_3^*[\text{MPa}] = a + b' \bullet \log(Q') + c \bullet b + d \bullet \log(p)$	3
9	$\sigma_3^*[\text{MPa}] = a + b' \bullet \log(Q') + c \bullet (b) + d \bullet \sigma_3$	3

$$\text{RSS} = \sum_{i=1}^{n} \left(y_i - \hat{y}_i\right)^2, \tag{14}$$

where i is the index that covers the total number of cases, n is the total number of simulated cases, y_i is the minimum principal stress of the simulated cases considering the empirical ELOS, and $\hat{y}_i$ is the minimum principal stress estimated by the evaluated criterion. Next, the proposed criteria are analysed according to the adjusted coefficient of determination ($\bar{R}^2$), given by Eq. (15):

$$\bar{R}^2 = 1 - \left(1 - R^2\right)\left(\frac{n-1}{n-(k+1)}\right), \tag{15}$$

where R^2 is the coefficient of determination, n is the total number of data, and k is the number of independent variables. In this case, the coefficient of determination is given by Eq. (16):

Table 4 Correlation coefficients between the considered variables

	Q'	σ_1^{wall}[MPa]	σ_2^{wall}[MPa]	σ_3^{wall}[MPa]	σ_3^*[MPa]	b	p
Q'	1						
σ_1^{wall}[MPa]	− 0.56	1					
σ_2^{wall}[MPa]	− 0.22	0.34	1				
σ_3^{wall}[MPa]	− 0.17	− 0.09	0.50	1			
σ_3^*[MPa]	− 0.68	0.50	0.54	0.46	1		
b	0.26	− 0.29	0.57	− 0.01	− 0.03	1	
p	− 0.51	0.75	0.80	0.52	0.71	0.02	1

Table 6 Summary of fitted criteria and adjusted coefficients of determination

Criterion number	Criterion	$\bar{R}^2$
0a	$\sigma_3^*[\text{MPa}] = 0$	0.00
0b	$\sigma_3^*[\text{MPa}] = \sigma_{t-\text{average}}$	0.22
1	$\sigma_3^*[\text{MPa}] = 2.07 - 2.92 \bullet \log(Q')$	0.69
2	$\sigma_3^*[\text{MPa}] = 2.71 - 3.15 \bullet \log(Q') - 0.07 \bullet \sigma_1$	0.71
3	$\sigma_3^*[\text{MPa}] = 1.23 - 2.60 \bullet \log(Q') + 0.39 \bullet \sigma_2$	0.79
4	$\sigma_3^*[\text{MPa}] = 2.32 - 2.71 \bullet \log(Q') + 0.37 \bullet \sigma_3$	0.79
5	$\sigma_3^*[\text{MPa}] = 2.17 - 2.65 \bullet \log(Q') + 0.02 \bullet \sigma_1 + 0.38 \bullet \sigma_3$	0.79
6	$\sigma_3^*[\text{MPa}] = 1.56 - 3.12 \bullet \log(Q') + 1.93 * b$	0.73
7	$\sigma_3^*[\text{MPa}] = 0.82 - 2.24 \bullet \log(Q') + 2.29 \bullet \log(p)$	0.76
8	$\sigma_3^*[\text{MPa}] = 0.57 - 2.46 \bullet \log(Q') + 1.47 \bullet b + 2.03 \bullet \log(p)$	0.78
9	$\sigma_3^*[\text{MPa}] = 1.83 - 2.90 \bullet \log(Q') + 1.82 \bullet b + 0.36 \bullet \sigma_3$	0.82

Table 7 Input data for mesh sensitivity analysis

Simulated case	
Depth [m]	778.4
Dip [°]	60.9
Width [m]	7.2
Length [m]	23.4
Height [m]	33.3
Aspect ratio (H/L)	1.6
Hydraulic radius, HR [m]	7.2
Rock mass quality, Q'	7.4
Stability number, N	11.7
Modulus of deformation, Erm [GPa]	32.2

$$R^2 = 1 - \left(\frac{\sum_{i=1}^{n} \left(y_i - \hat{y}_i\right)^2}{\sum_{i=1}^{n} \left(y_i - \bar{y}\right)^2} \right), \tag{16}$$

where $\bar{y}$ is the average value of the minimum principal stress of the simulated cases considering the empirical ELOS.

Table 6 shows the values of parameters (a, b', c, and d) and the adjusted coefficients of determination of the proposed criteria. Table 6 has the following implications:

- The lowest adjusted coefficient of determination is obtained for the conventional criteria ($\sigma_3 = 0$ [MPa] and $\sigma_3 = \sigma_t$).
- Including the rock mass quality (Q') directly in criterion number 1 significantly improves the adjusted coefficient of determination.
- Criteria 3, 4, and 5 present an adjusted coefficient of determination of 0.79.
- The highest adjusted coefficient of determination is obtained for criterion number 9.

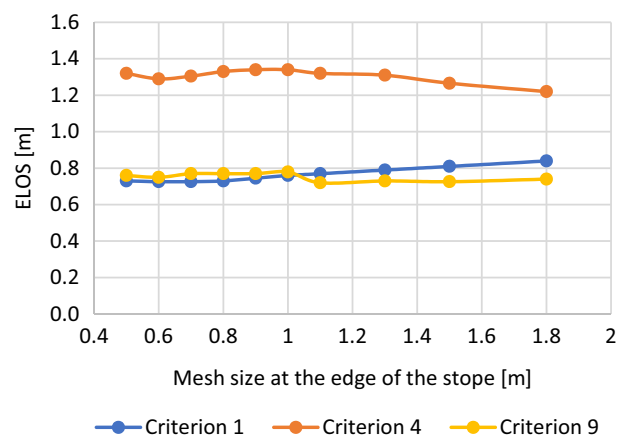

Fig. 10 Estimated ELOS from numerical modelling with criteria 1, 4, and 9 and the sensitivity to the mesh size

- The best criteria are number 4 and number 9. From these criteria, it can be observed that the rock mass quality and parameters b and σ_3 have a great influence when estimating the target minimum principal stress (σ_3^*).

3.2 Mesh sensitivity

A mesh sensitivity analysis is defined to study the behaviour of the proposed criteria. In this case, the mesh size at the edge of the stope varies from 0.5 to 1.8 [m]. For practical purposes, only three criteria are considered: numbers 1, 4, and 9, given the different variables that each one considers.

A synthetic case of an open stope is modelled. Table 7 shows the input parameters used in this case. It should be noted that this information corresponds to the average value of the empirical database studied.

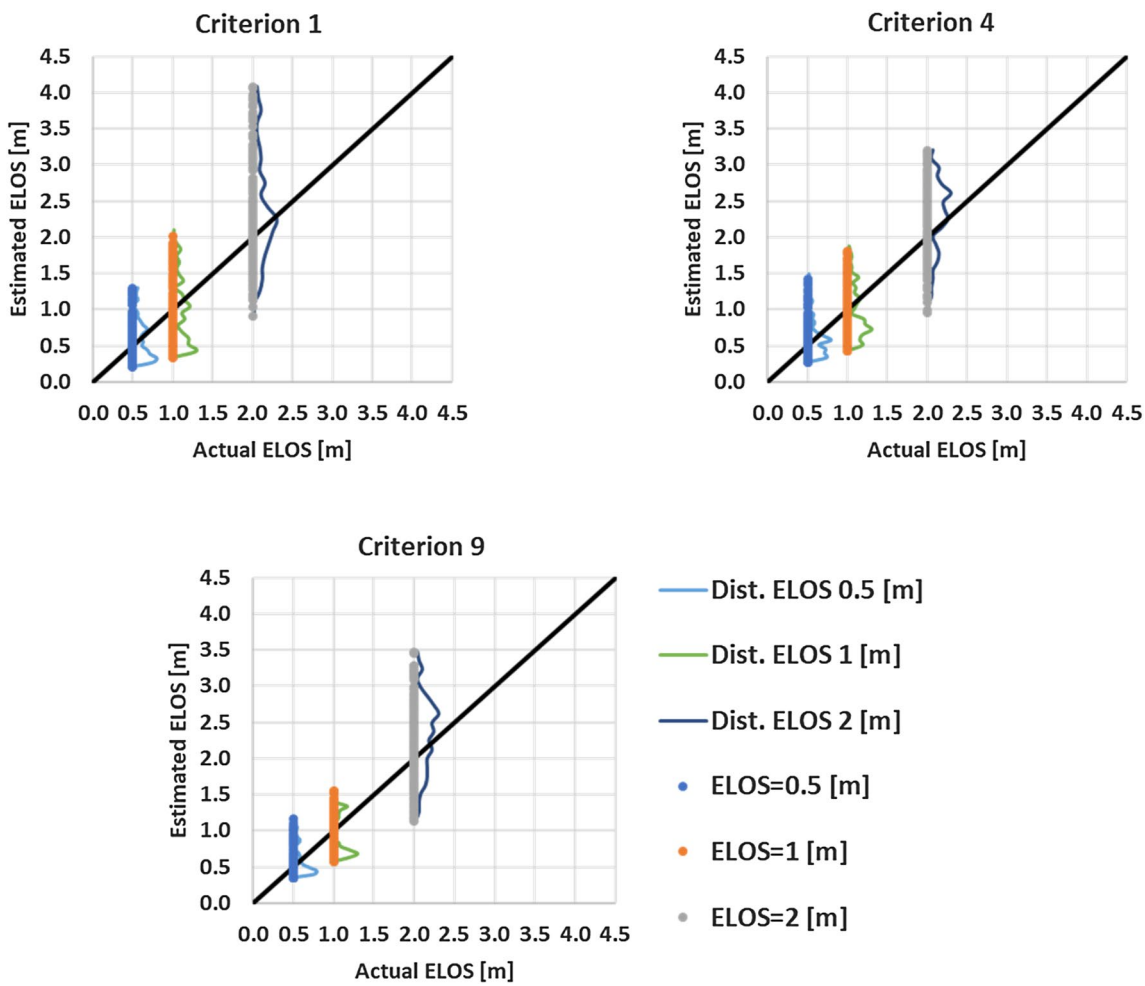

Fig. 11 Comparison between the estimated ELOS and the empirical ELOS for criteria 1, 4, and 9. The distribution of the numerical results obtained for each case is included as the curve that projects from the vertical line for each empirical ELOS

Figure 10 presents the ELOS generated by the σ_3^* calculated for each criterion. It can be observed that each criterion is mostly insensitive to the mesh size, given that the calculated ELOS does not vary by more than 0.1 [m] from the average.

3.3 Criteria performance

For practical comparison purposes, criteria 1, 4, and 9 are studied. Figure 11 shows the performance of each criterion to estimate the ELOS in different cases. It should be noted that the data used in this study were the same data used to fit the overbreak criterion, that is, the cases with ELOS 0.5, 1, and 2 m (Fig. 4). Each graph shows a comparison between the ELOS estimated by the corresponding criterion and the empirical ELOS. For each empirical ELOS, the distribution of the numerical results obtained for each case (curve that projects from the vertical line for each empirical ELOS) is presented. A diagonal line is incorporated into the graphics to indicate a perfect fit between the estimated and empirical ELOS.

Criterion number 1 presents a large spread of results (long vertical line), which is consistent with the adjusted R^2 presented earlier (Table 6). Criterion 9 presents a lower spread and more precise results than those of criterion 4, which is directly related to the $\bar{R}^2$. From the distributions shown, criteria 1 and 4 have erratic performances in estimating the ELOS of 0.5 and 1 [m]. For the ELOS of 2 [m], the three criteria concentrate their results around this value; however, they tend to overestimate this overbreak value.

The addition of the aspect ratio as a parameter to represent the geometry of the stopes allows incorporating into the analysis a factor used in previous works (Suorineni 1998; Suorineni et al. 1999; Henning and Mitri 2007). In this manner, Fig. 12 shows the performance of each criterion to estimate the empirical ELOS as a function of the aspect ratio. Figure 12a shows the performance of the three criteria used

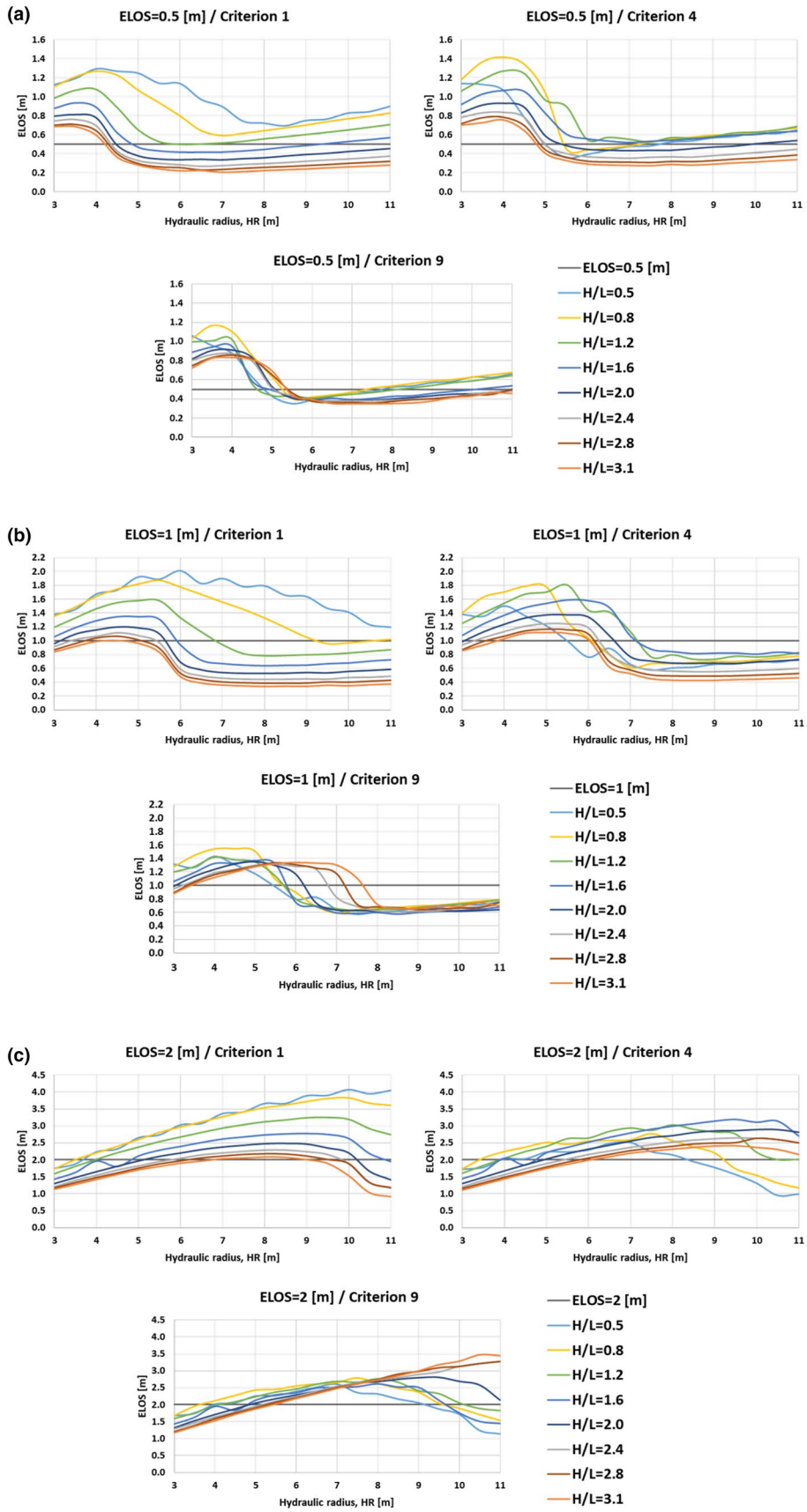

Fig. 12 Performance of each criterion for estimating the empirical ELOS as a function of the aspect ratio. **a** ELOS of 0.5 [m], (**b**) ELOS of 1 [m], and (**c**) ELOS of 2 [m]

Table 8 Global and local bias of each criterion for estimating the empirical ELOS

	Bias			
	Global	ELOS 0.5 [m]	ELOS 1 [m]	ELOS 2 [m]
Criterion 1	0.32	0.09	0.22	0.67
Criterion 4	0.18	0.08	0.14	0.32
Criterion 9	0.17	0.04	0.10	0.36

to estimate the empirical ELOS of 0.5 [m]. When the aspect ratio varies from 0.5 to 3.1, criteria 1 and 9 have the highest and lowest deviation, respectively. Criterion 1 tends to overestimate the ELOS when the aspect ratio is lower than 1.6 and tends to underestimate the ELOS when the aspect ratio is higher than or equal to 1.6. Criterion number 4 tends to overestimate the ELOS when the hydraulic radius is lower than 5 [m] independent of the value of the aspect ratio and tends to underestimate the ELOS when the HR is higher than 5.5 [m] for an aspect ratio higher than 1.6. It can be observed that criterion number 9 is invariant to the aspect ratio variation when estimating the ELOS of 0.5 [m]. This criterion tends to overestimate the ELOS when the HR is lower than 5 [m] and tends to underestimate the ELOS when the HR is higher than or equal to 5.5 [m].

Figure 12b presents the performance of the three criteria used to estimate the empirical ELOS of 1 [m]. Criterion number 1 has the highest deviation, while criterion number 9 has the lowest deviation when estimating the ELOS of 1 [m] as a function of the aspect ratio. Criterion 1 tends to overestimate this ELOS of 1 [m] when the aspect ratio is lower than 1.2 and tends to underestimate it when the ratio is higher than 1.6. Criterion 4 tends to overestimate the ELOS when the HR is lower than 7 [m] and tends to underestimate it when it is higher than or equal to 7 [m]. Criterion number 9 has a similar performance to that of criterion number 4 as a function of the aspect ratio. This criterion tends to overestimate the ELOS when the HR is lower than 6 [m] and tends to underestimate it when the HR is higher than or equal to 6 [m]. It can be noted that this criterion has a special behaviour when the HR is between 6 and 8 [m] given the aspect ratio values of the hangingwall.

Figure 12c shows the performance of the three criteria used to estimate the empirical ELOS of 2 [m]. Criterion number 1 has the highest deviation, while criterion number 9 has the lowest deviation. Criterion number 1 tends to overestimate the ELOS except when the HR is lower than 5 [m]. Criterion number 4 tends to overestimate the ELOS when the value of the hydraulic radius increases. Criterion number 9 has a similar behaviour to that of criterion 4, but when the HR is higher than 9 [m] and the aspect ratio is lower than or equal to 1.6, it tends to underestimate the ELOS.

From the graphs described above, it can be concluded that the three criteria have different performances for estimating the different ELOS values studied in this paper. Criterion number 9 has the lowest variation when estimating each empirical ELOS value, but it equally tends to overestimate and underestimate the dilution under certain HR and aspect ratio values. It is important to note that the range of the aspect ratio used in this study is limited to the range present in the database used. This range can be extended in future works to provide a more comprehensive study of this criterion with respect to the aspect ratio.

Next, the bias of each criterion is calculated. Equation (17) is used for this purpose:

$$\text{Bias} = \frac{\sum \left(y - \hat{y}\right)^2}{n - (k+1)} \tag{17}$$

where y is the estimated value for each criterion, $\hat{y}$ is the average of the real data, n is the total number of data, and k is the number of independent variables.

Table 8 shows the global and local bias for each criterion. It can be observed that criterion 9 has a lower global bias than that of criteria 1 and 4. Criterion 9 has a lower bias for estimating the ELOS of 0.5 and 1 [m] than that of criteria 1 and 4; however, when estimating the ELOS of 2 [m], criterion 4 is the one that has the better performance.

Next, the proposed criteria 1, 4, and 9 are used to estimate hangingwall overbreak and to compare the results with the empirical updated ELOS curves. For this, 56 new cases are modelled numerically. These cases represent the ordered pairs of HR and N obtained from the stability graph. Figure 13 shows the estimated ELOS of each criterion compared with the empirical updated ELOS curves (Castro 2015). It can be observed that criterion number 1 tends to overestimate the overbreak between the ELOS curves of 1 [m] and 2 [m]. Criterion number 4 tends to follow the ELOS lines; nevertheless, when $N = 20.8$, this criterion tends to overestimate the hangingwall overbreak at lower HR values (less than 4 [m]) and tends to underestimate the hangingwall overbreak at higher HR values (greater than 7 [m]). Criterion 9 best reproduces the empirical updated ELOS curves.

Finally, Fig. 14 shows the behaviour of the proposed criterion 9 as a function of the adjusted stress variables estimated at the centre of the hangingwall, b, σ_3, and the quality of the rock mass, Q'. For this analysis, one of the parameters is considered variable, while the others remain constant. In this manner, the impact of each variable on the behaviour of the proposed criterion can be analysed individually.

Figure 14 has the following implications:

- As the value of the stress variable b increases, the σ_3^* value increases (Fig. 14a). This is an effect of the intermediate principal stress, which increases the

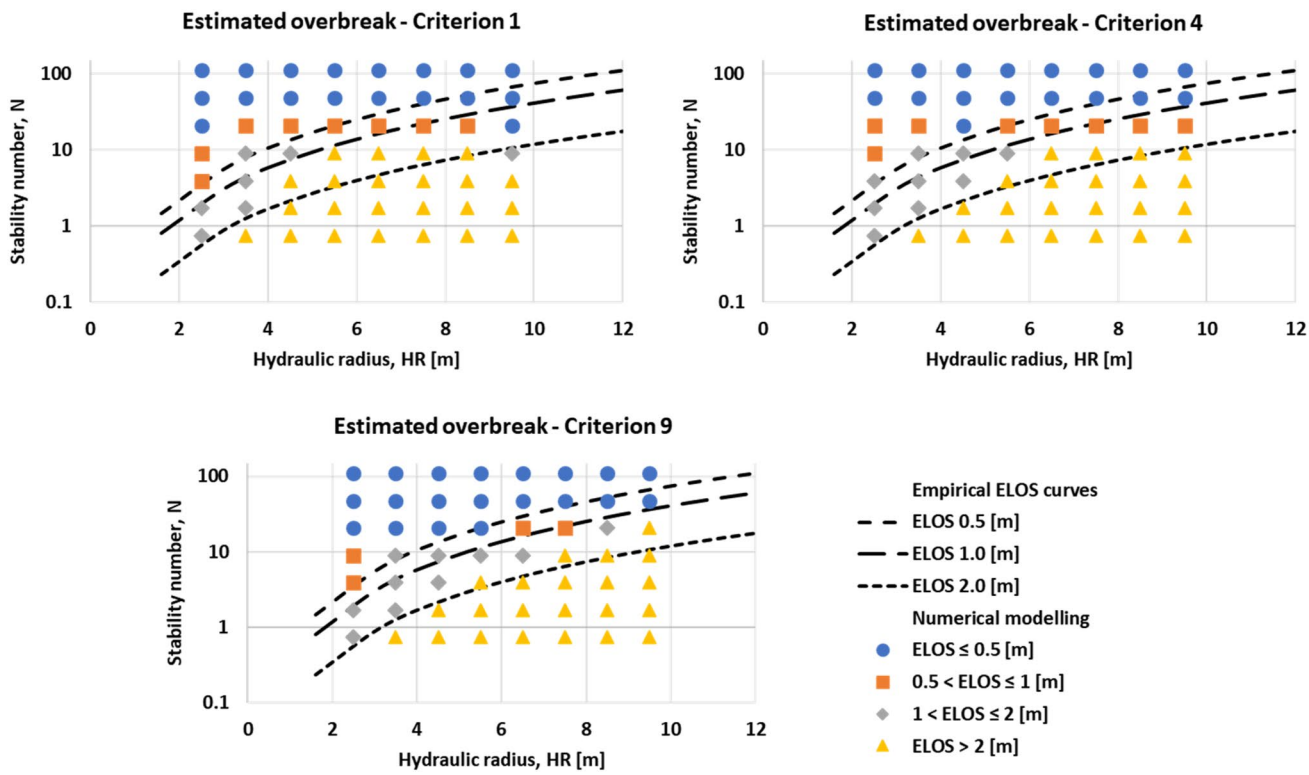

Fig. 13 Comparison of the ELOS estimated with the proposed criteria 1, 4, and 9 with the empirical updated ELOS curves

hangingwall confinement and, therefore, the stability of the wall.

- As the value of the minor principal stress (σ_3) in the hangingwall increases, the σ_3^* value increases (Fig. 14b). This result is related to the value of the σ_3^* that must be larger than the value of σ_3 at the centre of the hangingwall to estimate the overbreak correctly.
- As the value of the rock mass quality Q' increases, the σ_3^* value decreases (Fig. 14c). The hangingwall overbreak must be lower with a better rock quality for the same stress conditions.

3.4 Verification of the criterion

The cases from the collected empirical database (Table 2) that present complete information for all the variables are used to verify the generality of the proposed criterion. A total of 30 cases presented complete information. Figures 15 and 16 present the histogram and cumulative percentage for the different variables related to the intact rock, rock mass properties, geometry, depth, and in situ stress conditions. From Figs. 15 and 16, it can be observed that the cases used to verify the criterion are significantly different from the cases used to calibrate the criterion.

Next, each of the cases is simulated, and the principal stresses (σ_1, σ_2, σ_3) are determined at the centre of the stope hangingwall (Fig. 9). Then, the overbreak isocontour (σ_3^*) is determined using criterion 9. Finally, the volume and corresponding ELOS associated with the overbreak isocontour are estimated. Figure 17 presents the histogram and the cumulative percentage for the difference between the $ELOS_{measured}$ available from the database and the $ELOS_{estimated}$ by the proposed criterion. It can be observed that, 93% and 80% of the cases, have $ELOS_{measured}$–$ELOS_{estimated}$ lower than 0.5 and 0.2 [m], respectively. The results of the model provide a reasonable fit to the data measured in the field.

4 Case study

To illustrate the applicability of the proposed criterion 9, a case study is presented using the data published by Martin et al. (1999). This case corresponds to a mine operated by long-hole stoping in a narrow vein operation in Canada, with 3 [m]-wide open stopes at a depth of 300 [m]. Field observations had noted that dilution became excessive beyond a stope strike length of approximately 25 [m] with stope heights ranging from 20 to 40 [m], that is, an hydraulic radius close to 5 [m] and 8 [m] for the cases of 20 [m] and 40 [m] heights, respectively.

In this case, stopes of 20, 40, and 60 [m] heights are modelled with strike lengths between 10 and 60 [m]. This

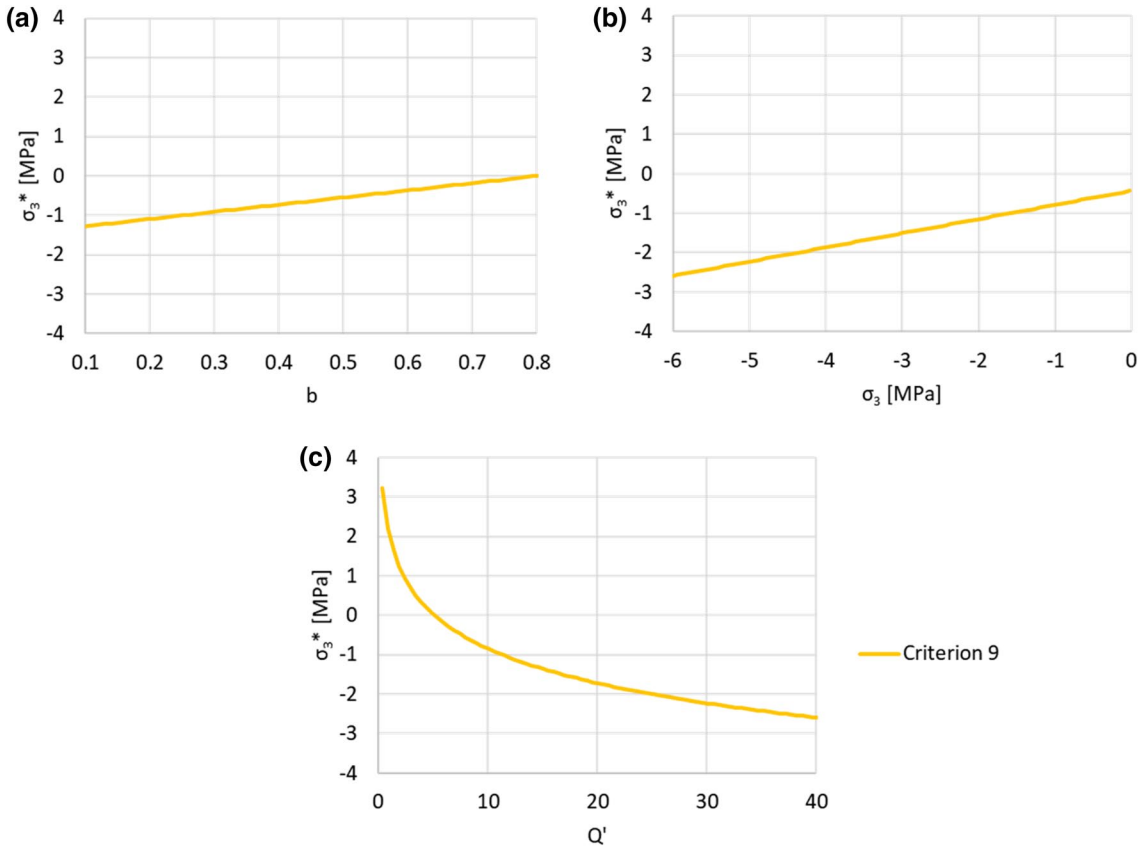

Fig. 14 Behaviour of the proposed criterion 9 as a function of the adjusted variables. **a** Impact of the stress variable b. **b** Impact of the minor principal stress, σ_3. **c** Impact of the quality of the rock mass, Q'

geometry allows the evaluation of open stopes with a hydraulic radius between 3.3 and 15 [m]. In each case, the estimated overbreak is estimated from the numerical model using criterion number 9, and the result is compared with the case history presented by Martin et al. (1999). A summary of the geometry, rock mass quality, and in situ stress used in these cases is shown in Table 9.

Figure 18 shows the estimated ELOS for open stopes of 20, 40, and 60 [m] height for the simulated study case using the proposed criterion (solid lines). This figure includes the estimated ELOS using the σ_3=0 [MPa] criterion (dotted lines) and the recorded field values of two case histories presented by Martin et al. (1999) identified as "Measured values". The two case histories correspond to stopes of 25 [m] and 40 [m] height. It can be observed that the proposed criterion correctly estimates the field observations mentioned above. The estimated ELOS curve for a stope height of 20 and 40 [m] presents an increase in overbreak for HRs close to 5 and 8 [m], respectively.

Figure 18 indicates that the proposed criterion tends to overestimate the measured overbreak. This is an effect of the average case used in the numerical models to calibrate the criterion. The hangingwall of the average case has a dip of 60.9°, resulting in a more unfavourable stability condition than the one reported in the cases presented by Martin et al. (1999) with a dip equal to 90°.

From Fig. 18, it can be observed that for criterion number 9 and σ_3=0 [MPa], the stopes of 20 [m] height present a higher estimated overbreak than the 40 and 60 [m] height stopes. This is an effect of the stress distribution around the excavation related to the height/length ratio of the hangingwall. In the case of the 20 [m] height stope, the ratio is less than or close to 1, which generates a more unstable condition. This can also be observed when comparing the estimated ELOS curves for stopes of 40 [m] and 60 [m] height. This finding will be explored further in the discussion section.

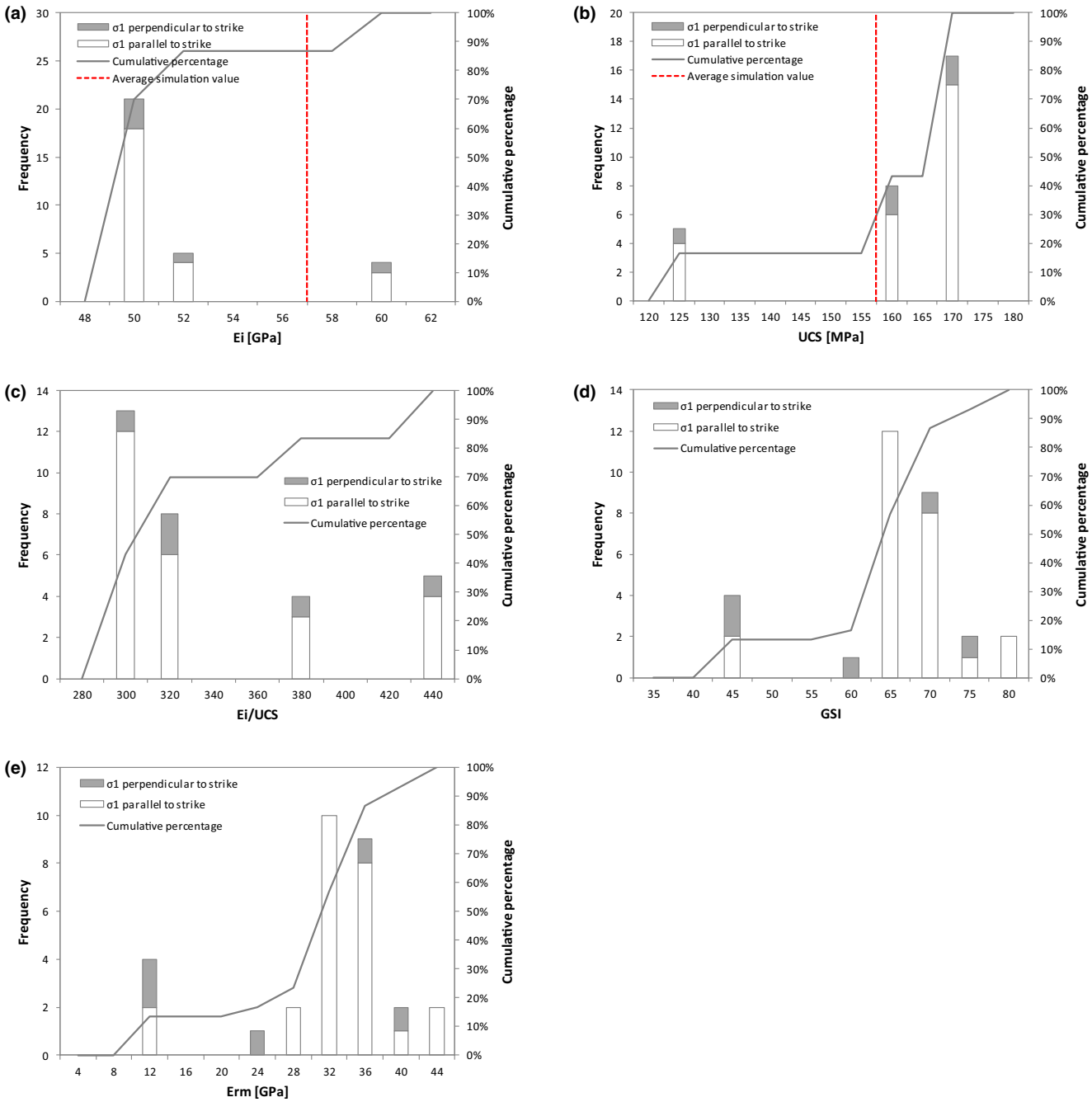

Fig. 15 Histograms and cumulative percentage of cases from the empirical database with complete information to be used for verification of the overbreak criterion (30 cases). The vertical dotted line indicates the average values of the variables used to calibrate the criterion. The orientation of the strike of the stopes relative to the orientation of the major principal stress is indicated. **a** Intact rock Young´s modulus. **b** Uniaxial compressive strength. **c** Ratio between the Young´s modulus and the uniaxial compressive strength. **d** Geological strength index. **e** Rock mass Young´s modulus

5 Discussion

The correlation analysis demonstrates that the best variables to calibrate a criterion for the numerical modelling of hangingwall overbreak in open stopes are the rock mass quality Q', the minor principal stress σ_3, and the stress variable b. This is a result of the low probability of linear combinations between these parameters.

The proposed criterion (number 9) has a significantly better performance than that of the criteria traditionally used in the industry (σ_3=0 [MPa] and $\sigma_3 = \sigma_t$) to estimate

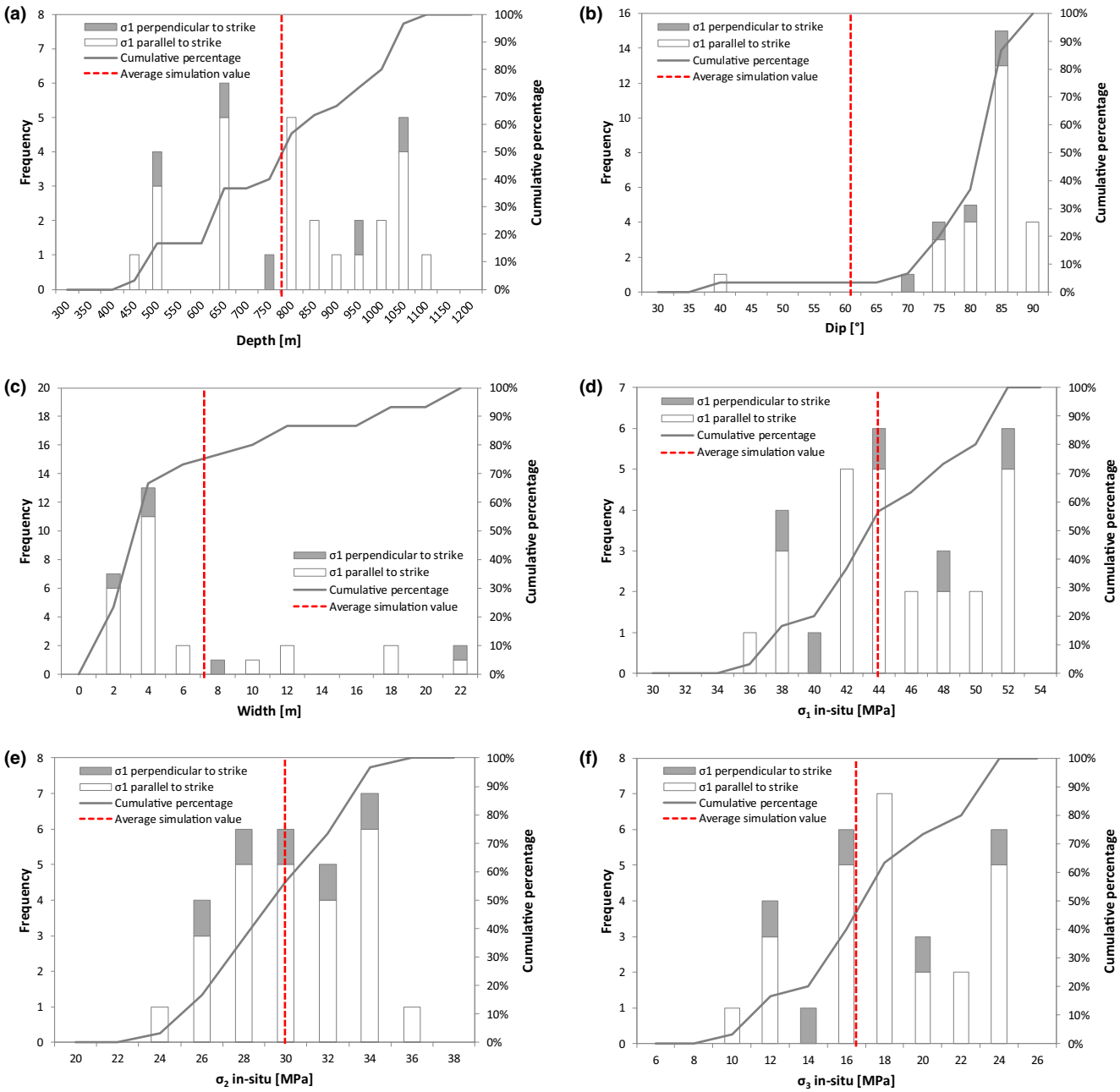

Fig. 16 Histograms and cumulative percentage of cases from the empirical database with complete information to be used for the verification of the overbreak criterion (30 cases). The vertical dotted line indicates the average values of the variables used to calibrate the criterion. The orientation of the strike of the stopes relative to the orientation of the major principal stress is indicated. **a** Depth. **b** Dip. **c** Width. **d** Major in situ principal stress. **e** Intermediate in situ principal stress. **f** Minor in situ principal stress

the overbreak in open stope hangingwalls. The main reasons are as follows:

- The new criterion directly considers the impact of the quality of the rock mass in the hangingwall overbreak.
- The new criterion considers the impact of stope geometry through the principal stress distribution around the stope. Specifically, the impact of the intermediate principal stress (σ_2) and the minimum principal stress (σ_3) in the rock mass confinement is considered.

The addition of these new variables provides a more comprehensive criterion than those currently used and better distinguishes between different conditions of the stope design and rock mass. The proposed criterion considers the impact

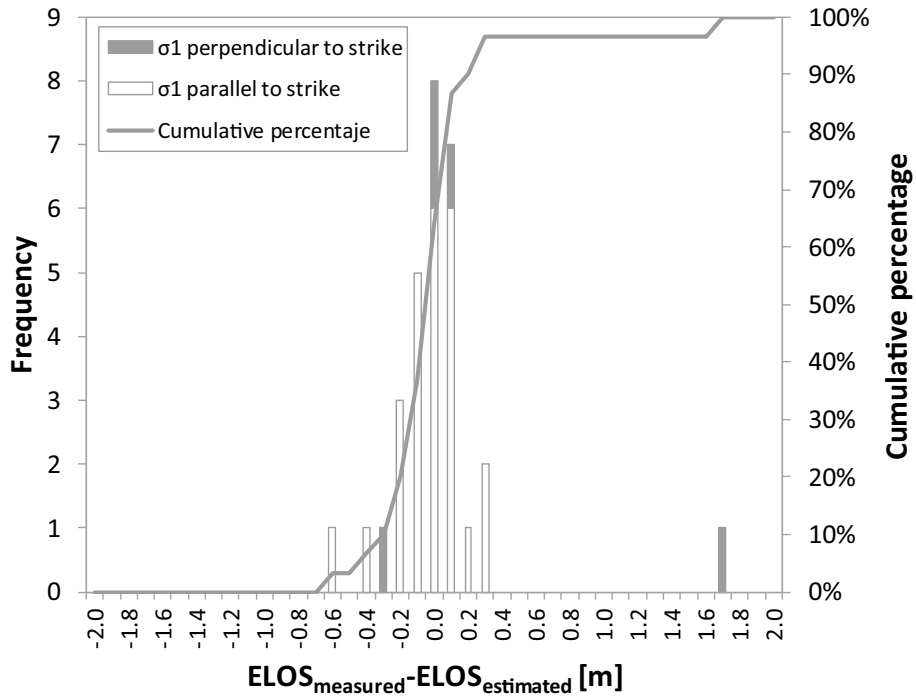

Fig. 17 Histogram and cumulative percentage for the difference between the $ELOS_{measured}$ available from the database and the $ELOS_{estimated}$ by the proposed criterion

Table 9 Summary of the geometry, rock mass quality, and in situ stress for the study case (Martin et al. 1999)

Simulation parameters	
Depth [m]	300
Width [m]	3
Dip [°]	90
Height [m]	20, 40, 60
Length [m]	10 to 60
Q'	18
GSI	70
E [GPa]	35
N	0.2
UCS_{rm} [MPa]	22.3
σ_{trm} [MPa]	− 0.8
$\sigma_{1-insitu}$[MPa]	22
$\sigma_{2-insitu}$[MPa]	13
$\sigma_{3-insitu}$[MPa]	8

of rock mass quality (Stewart 2005), the impact of stress relaxation (Clark 1998; Suorineni 1998; Diederichs and Kaiser 1999; Henning and Mitri 1999; Martin et al. 1999; Wang et al. 2002b; Stewart and Trueman 2003, 2004; Henning and Mitri 2007), and the influence of the intermediate principal stress (Stewart and Trueman 2004) on stope stability.

Criterion number 9 presents a low dispersion of results with ELOS estimates of 0.5 [m], 1 [m], and 2 [m]. According to the distribution of estimated ELOS values obtained for this criterion, it was found that most of the estimated values are close to the actual value, which is indicated by the goodness of fit between the variables used and the prime minimum principal stress (σ_3^*). By varying the aspect ratio of the stopes, it was found that the best criterion remained near constant when estimating an ELOS of 0.5 [m], 1 [m], and 2 [m], which indicates that this criterion is not affected by variations in the ratio between the height and length of the stope. However, it is affected by variations in the hydraulic radius due to the influence of this parameter on the stress distribution around the excavation.

It was shown that the proposed criterion offers sufficient flexibility to be applied to a wide range of geometries, in situ stress conditions, and depth and rock mass properties. It should be noted that the proposed criterion does not consider rockbursting conditions that could occur in deep underground mines, so it should be used with caution in these cases.

Stopes with heights lower than their length (i.e., *H*/*L* less than 1) have a stress distribution that is more unfavourable for hangingwall stability, because σ_1 is perpendicular to the strike stope and tends to be distributed vertically around the excavation. This is related to the effect of the intermediate principal stress. Figure 19 illustrates this situation.

The results of the case study presented in this paper show that the $\sigma_3 = 0$ [MPa] criterion tends to underestimate the measured values, because only the σ_3 distribution around the stopes is considered. This criterion does not correctly estimate the field observations for stopes higher than 20 [m], because it shows an increase in overbreak for hydraulic radius close to 7 [m] instead of 8 [m] for 40 [m] height stopes. On the other hand, criterion number 9 tends to overestimate the measured values of the history cases

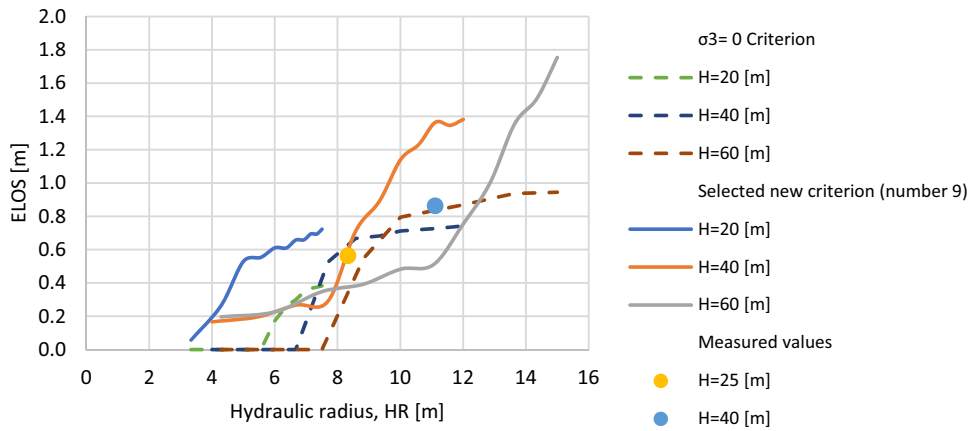

Fig. 18 Estimated ELOS for 20, 40, and 60 [m] height open stopes for the simulated study case using the proposed criterion (solid lines) and σ_3=0 [MPa] criterion (dotted lines). The measured field values of two case histories presented by Martin et al. (1999) for 25 and 40 [m] height stopes are included

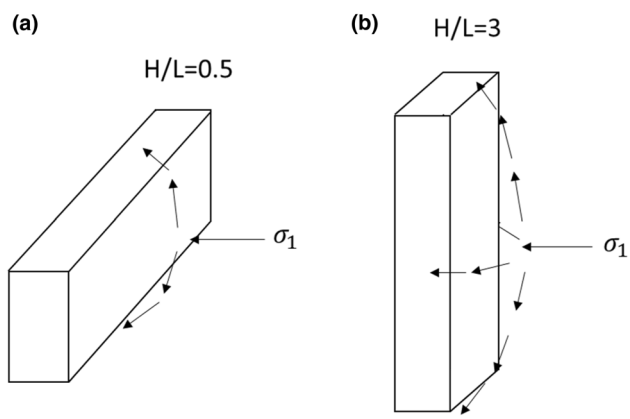

Fig. 19 Principal stress distribution in (**a**) stopes with H/L less than 1 and (**b**) stopes with H/L greater than 1

published by Martin et al. (1999), because it was calibrated using a lower hangingwall dip than that of the recorded cases. However, the proposed criterion correctly estimates the field observations, because it shows an increase in overbreak for hydraulic radius close to 5 [m] for 20 [m] height stopes and for hydraulic radius close to 8 [m] for 40 [m] height stopes.

Given the results, it can be concluded that criterion number 9 proposed in this paper is a reasonable tool for estimating overbreak in hangingwall stopes.

The main advantages and considerations of the proposed criterion are as follows:

- It can be used in three-dimensional numerical modelling.
- It directly relates the stress distribution around the stope with the rock mass quality, which gives more accurate results when different conditions are evaluated.
- It can be used in early engineering stages to estimate the unplanned dilution that allows updating the tonnage to extract, its grade, and the value of processing.
- It fits well with empirical estimation guides that are currently used to estimate the hangingwall overbreak, which allows us to complement the empirical methods with numerical modelling.
- The proposed methodology can be used to calibrate the criterion with any available empirical database.

6 Conclusions

In this paper, a three-dimensional numerical study is used to calibrate a new criterion for estimating hangingwall overbreak. Several numerical models of open stopes are modelled considering different geometrical and geotechnical parameters. Multiple linear regressions are evaluated using the rock mass geotechnical properties and the principal stresses in the hangingwall as independent variables. The performance of each criterion is analysed according to the adjusted coefficient of determination and by comparing its results with the values used for its calibration.

Based on the numerical and adjustment analyses performed in this study, a new criterion for estimating hangingwall overbreak is proposed. The proposed criterion establishes a significant influence and relationship between rock quality and the minimum and intermediate principal stresses on hangingwall overbreak.

The use of the proposed criterion improves the predictive capabilities of the numerical modelling method and leads to a modification of the numerical analysis currently used in the industry. This modification implies changes in output information from numerical models, because it considers the three principal stresses at the centre of the hangingwall. It is important to note that once the parameters used in the proposed criterion are obtained, the same numerical model must be used to calculate the volume of rock that it is contained in the σ_3 isocontour calculated with the criterion.

The proposed criterion for estimating overbreak does not consider rockbursting conditions. At depth, the risk for rockbursting and major seismic events increases and thus typically becomes the criteria for stope sizing and not the stability graph method. Therefore, the proposed criterion must be used with caution when addressing deep underground mines.

The numerical modelling methodology presented in this paper has proven to be useful for developing a new numerical criterion and can be used to improve its performance considering new variable parameters.

Finally, the authors recommend developing a standardized database to improve the predictive capabilities of the empirical stability graph, which must be compared with numerical modelling to improve the stope design method. A standardized database is defined here as a combination of case histories from multiple sources that have been collected, processed, and analysed with a standardized procedure. With this objective, an integrated software program, MineRoc (Vallejos et al. 2015), was developed. MineRoc includes an acquisition platform or mine data and geotechnical information, a design module for stopes, and a back-analysis platform for calibrating a local stability graph curve. The application and benefits of MineRoc have been illustrated elsewhere for sublevel open stopes in Chilean mining operations (Vallejos et al. 2015, 2017b; Miranda et al. 2018).

Acknowledgements The authors gratefully acknowledge the financial support from basal project FB-0809 and CONICYT/PIA Project AFB180004 Advanced Mining Technology Center (AMTC). The FLAC3D software licenses provided by Itasca Chile Spa is also gratefully acknowledged.

Author contributions JAV and LD designed the study, performed the numerical simulations, analysed the results, and wrote the manuscript.

Funding This study was funded from basal project FB-0809 and CONICYT/PIA Project AFB180004 Advanced Mining Technology Center (AMTC).

Compliance with Ethical Standards

Conflict of interest Javier A. Vallejos declares that he has no conflict of interest. Leandro Díaz declares that he has no conflict of interest.

References

Amoussou CA, Vallejos JA, Trueman R (2020) Stability assessment of underground mine stopes subjected to stress relaxation. Min Technol 129:30–39. https://doi.org/10.1080/25726668.2020.1721995

Arjang B (1989) Pre-mining stresses at some hard rock mines in the Canadian Shield. In: The 30th US symposium on rock mechanics (USRMS). American Rock Mechanics Association, Morgantown, West Virginia

Bewick R, Kaiser P (2009) Numerical assessment of factor b in mathews method for open stope design. In: Diederichs M, Grasselli G (eds) Proceedings of the 3rd CANUS rock mechanics symposium. Toronto, Canada, pp 89–90

Capes GW (2009) Open stope hangingwall design based on general and detailed data collection in rock masses with unfavourable hangingwall conditions. University of Saskatchewan

Castro C (2015) Modelamiento numérico de la dilución por sobre excavación en minería subterránea explotada por sublevel stoping. Doctorial Thesis, Universidad de Chile

Cepuritis P, Villaescusa E (2006) Comprehensive back analysis techniques for assessing factors affecting open stope performance. In: Rock mechanics in underground construction: ISRM international symposium 2006: 4th Asian rock mechanics symposium, Singapore. World Science Pub. Co., Hacken, NJ, p 45

Chen DW, Chen JY, Zavokni ZM (1983) Stability analysis of sublevel open stopes at great depth. In: The 24th US symposium on rock mechanics (USRMS). American Rock Mechanics Association, College Station, Texas

Clark L, Pakalnis R (1997) An empirical design approach for estimating unplanned dilution from open stope hangingwalls and footwalls. In: Proceedings of the CIM 99th annual general meeting. Vancouver, Canada

Clark LM (1998) Minimizing dilution in open stope mining with a focus on stope design and narrow vein longhole blasting. Doctoral Dissertation, University of British Columbia

Deere DU, Hendron AJ, Patton FD, Cording EJ (1967) Design of surface and near surface construction in rock. In: Fairhurst C (ed) The 8th US symposium on rock mechanics (USRMS). American Rock Mechanics Association, New York, pp 237–302

Díaz L, Vallejos J, Castro C (2018) Revisión de métodos de estimación de sobre-excavación para caserones abiertos. In: Congreso iberoamericano en minería subterránea y a cielo abierto UMining. Santiago

Diederichs MS, Kaiser PK (1999) Tensile strength and abutment relaxation as failure control mechanisms in underground excavations. Int J Rock Mech Min Sci 36:69–96. https://doi.org/10.1016/S0148-9062(98)00179-X

El Mouhabbis HZ (2013) Effect of stope construction parameters on ore dilution in narrow vein mining. Doctoral Dissertation, McGill University Libraries

Hadjigeorgiou J, Leclair J, Potvin Y (1995) An update of the stability graph method for open stope design. CIM rock mechanics and strata control session. Halifax, Canada, pp 154–161

Heidarzadeh S, Saeidi A, Rouleau A (2018) Evaluation of the effect of geometrical parameters on stope probability of failure in the open stoping method using numerical modeling. Int J Min Sci Technol 29:399–408. https://doi.org/10.1016/j.ijmst.2018.05.011

Henning JG (2007) Evaluation of long-hole mine design influences on unplanned ore dilution. Doctoral Dissertation, McGill University Libraries

Henning JG, Mitri HS (1999) Examination of hanging-wall stability in a weak rock mass. CIM Bull 92:40–44. https://doi.org/10.1016/B978-008043013-3/50009-2

Henning JG, Mitri HS (2007) Numerical modelling of ore dilution in blasthole stoping. Int J Rock Mech Min Sci 44:692–703. https://doi.org/10.1016/j.ijrmms.2006.11.002

Henning JG, Mitri HS (2008) Assessment and control of ore dilution in long hole mining: case studies. Geotech Geol Eng 26:349–366

Hoek E, Carranza-Torres C, Corkum B (2002) Hoek-Brown failure criterion-2002 edition. In: Hammah R, Bawden W, Curran J, Telesnicki M (eds) Proceedings of the fifth North American rock materials symposium (NARMS-TAC), Univeristy of Toronto Press, Toronto, pp 267–273

Hoek E, Diederichs MS (2006) Empirical estimation of rock mass modulus. Int J Rock Mech Min Sci 43:203–215. https://doi.org/10.1016/j.ijrmms.2005.06.005

Hoek E, Kaiser PK, Bawden WF (1995) Support of underground excavations in hard rock. AA Balkema, Rotterdam

Hughes R (2011) Factors influencing overbreak in narrow vein longitudinal retreat mining. McGill University, Canada

Itasca Consulting Group (2018) FLAC3D v6

Jing L (2003) A review of techniques, advances and outstanding issues in numerical modelling for rock mechanics and rock engineering. Int J Rock Mech Min Sci 40:283–353. https://doi.org/10.1016/S1365-1609(03)00013-3

Larose D (2006) Data mining methods and models. Wiley-Interscience, Hoboken

Laubscher D, Taylor H (1976) The importance of geomechanics classification of jointed rock masses in mining operations. In: Proceedings of the symposium on exploration for rock engineering. AA Balkema, Cape Town, Johannesburg, pp 119–128

Laubscher DH (1994) Cave mining - the state of the art. J South Afr Inst Min Metall 94:279–293

Mah SG (1997) Quantification and prediction of wall slough in open stope mining methods. Doctoral Dissertation, University of British Columbia

Maloney S, Kaiser P, Vorauer A (2006) A re-assessment of in situ stresses in the Canadian Shield. In: Golden rocks 2006, The 41st US symposium on rock mechanics (USRMS). American Rock Mechanics Association, Alexandria

Martin CD, Kaiser PK, Tannant DD, Yazici S (1999) Stress path and instability around mine openings. In: 9th ISRM congress. International Society for Rock Mechanics and Rock Engineering, Paris, France

Mathews KE, Hoek E, Wyllie DC, Stewart SB (1981) Prediction of stable excavation spans for mining at depths below 1000 meters in hard rock. CANMET, Dublin

Mawdesley C (2002) Predicting rock mass cavability in block caving mines. Ph.D. Thesis, University of Queensland

Mawdesley C, Trueman R, Whiten WJ (2001) Extending the Mathews stability graph for open–stope design. Min Technol 110:27–39. https://doi.org/10.1179/mnt.2001.110.1.27

Miranda R, Vallejos J, Azorin J, Chavez D, Mondaca M, Garrido C, Catalan O (2018) Improving stopes stability limits using Mineroc software. In: Litvinenko V (ed) Geomechanics and geodynamics of rock masses. CRC Press, Florida, US, pp 569–576

Mitri H, Ma J, Mohammed MM, Bouteldja M (1998) Design of cable bolts using numerical modelling. In: da Silva A, et al. (eds) Design and construction in mining, petroleum and civil engineering. ISRM Regional Symposium, Beijing, pp 269–275

Mitri HS, Hughes R, Zhang Y (2011) New rock stress factor for the stability graph method. Int J Rock Mech Min Sci 1:141–145. https://doi.org/10.1016/j.ijrmms.2010.09.015

Nickson SD (1992) Cable support guidelines for underground hard rock mine operations. Doctoral Thesis, The University of British Columbia

O'Hara TA (1980) Quick guides to the evaluation of orebodies: risk analysis in mining. CIM Bull 73:87–99

Pakalnis R, Poulin R, Hadjigeorgiou J (1996) Quantifying the cost of dilution in underground mines. Int J Rock Mech Min Sci Geomech Abstr 5:233A

Pakalnis RC (1986) Empirical stope design at ruttan mine. PhD Thesis, University of British Columbia

Papaioanou A, Suorineni FT (2016) Development of a generalised dilution-based stability graph for open stope design. Min Technol 125:121–128

Potvin Y (1988) Empirical open stope design in Canada. Doctoral Dissertation, University of British Columbia

Sainsbury B, Sainsbury D, Vakili A (2015) Discrete analysis of open stope stability. In: Potvin Y (ed) Proceedings of the international seminar on design methods in underground mining, Australian Centre for Geomechanics, Perth, pp 79–94

Scoble M, Moss A (1994) Dilution in underground bulk mining: implications for production management. Geol Soc Lond Special Publ 79:95–108. https://doi.org/10.1144/GSL.SP.1994.079.01.10

Stewart P, Trueman R (2001) The extended mathews stability graph: quantifying case history requirements and site-specific effects. International symposium on mining techniques of narrow-vein deposits. CiteSeerX, Princeton, pp 85–92

Stewart P, Trueman R (2003) Applying the extended mathews stability graph to stress relaxation, site specific effects and narrow vein stoping. In: Hebblewhite BK (ed) 1st Australasian ground control in mining conference-ground control in mining: technology and practice. University of New South Wales, Australia, pp 55–61

Stewart PC (2005) Minimising dilution in narrow vein mines. Doctorial Thesis, University of Queensland

Stewart PC, Trueman R (2004) Quantifying the effect of stress relaxation on excavation stability. Min Technol 113:107–117. https://doi.org/10.1179/037178404225004986

Stewart PC, Trueman R (2008) Strategies for minimising and predicting dilution in narrow-vein mines–NVD Method. Narrow vein mining conference 2008. The Australasian Institute of Mining and Metallurgy, Victoria, pp 153–164

Stewart S, Forsyth W (1995) The Mathew's method for open stope design. CIM Bull 88:45–53

Suorineni F, Kaiser P, Tannant D (2001) Likelihood statistic for interpretation of the stability graph for open stope design. Int J Rock Mech Min Sci 38:735–744. https://doi.org/10.1016/S1365-1609(01)00033-8

Suorineni F, Papaioanou A, Baird L, Hines D (2016) A dilution-based stability graph for open stope design. In: Proceedings of the 7th international conference and exhibition on mass mining, The Australasian Institute of Mining and Metallurgy, Sydney, pp 511–522

Suorineni FT (1998) Effect of faults and stress on open stope design. PhD Thesis, University of Waterloo

Suorineni FT (2010) The stability graph after three decades in use: experiences and the way forward. Int J Min Reclam Env 24:307–339

Suorineni FT, Tannant DD, Kaiser PK (1999) Determination of fault-related sloughage in open stopes. Int J Rock Mech Min Sci 36:891–906. https://doi.org/10.1016/S0148-9062(99)00055-8

Tannant D, Diederichs M (1997) Cablebolt optimization in #3 mine. Kidd Mines Division, Timmins

Trueman R, Mawdesley C (2003) Predicting cave initiation and propagation. CIM Bull 96:54–59

Trueman R, Mikula P, Mawdesley C, Harries N (2000) Experience in Australia with the application of the Mathew's method for open stope design. CIM Bull 93:162–167

Vallejos JA, Miranda O, Gary C, Delonca A (2015) Development of an integrated platform for stability analysis and design in sublevel stoping mines—MineRoc®. In: Proceedings of the international seminar on design methods in underground mining. Australian Centre for Geomechanics, Perth, pp 477–488

Vallejos JA, Delonca A, Fuenzalida J, Burgos L (2016) Statistical analysis of the stability number adjustment factors and implications for underground mine design. Int J Rock Mech Min Sci 100:104–112. https://doi.org/10.1016/j.ijrmms.2016.06.001

Vallejos JA, Delonca A, Perez E (2017a) Three-dimensional effect of stresses in open stope mine design. Int J Min Reclam Env 32:355–374. https://doi.org/10.1080/17480930.2017.1309833

Vallejos JA, Miranda R, Burgos L, Perez E (2017b) Development of new design tools for open stoping underground mines. In: 51st US rock mechanics/geomechanics symposium, American Rock Mechanics Association, California

Wang J, Milne D, Yao M, Allen G (2002) Quantifying the effect of hangingwall undercutting on stope dilution. CIM AGM Vancouver, British Columbia

Wang J, Milne D, Wegner L, Reeves M (2007) Numerical evaluation of the effects of stress and excavation surface geometry on the zone of relaxation around open stope hangingwalls. Int J Rock Mech Min Sci 44:289–298. https://doi.org/10.1016/j.ijrmms.2006.07.002

Wang LG, Yamashita S, Sugimoto F, Pan C, Tan G (2003) A methodology for predicting the in situ size and shape distribution of rock blocks. Rock Mech Rock Eng 36:121–142. https://doi.org/10.1007/s00603-002-0039-8

Yao X, Allen G, Willett M (1999) Dilution evaluation using cavity monitoring system at HBMS—trout lake mine. In: Proceeding of the 101st CIM annual general meeting, Calgary

Publisher's Note Springer Nature remains neutral with regard to jurisdictional claims in published maps and institutional affiliations.